Publ. Natl. Astron. Obs. Japan Vol. 7. 1–24 (2003)

Chromospheric Structure Derived from Flash Spectra of the Total Solar Eclipse

Mitsugu MAKITA*

(Received September 30, 2002)

Abstract

A chromosphere model for the analysis of emission lines in a flash spectrum is constructed. Emission gradients of metallic and Balmer lines in flash spectra give height distributions of the total hydrogen and the product of electron and proton density in the high chromosphere, respectively. The derived distributions imply the presence of "spicule" structure which has a filling factor of 0.05 at 4,000 km above the base of the chromosphere. They explain the averaged eclipse curves of Ca II H and K, and Hε line profiles observed in a 1958 flash spectrum and the Balmer and Sr II emissions observed in a 1962 flash spectrum. Their excitation and ionization seem to match the radiation field of the chromosphere. They are applied to 24 Ca II H and K spicules in the higher chromosphere observed during the 1958 eclipse. The analysis shows that they have a turbulence of 22 km/s on the average and 19 of them are thinner than 2,000 km. The Ca II H and K, and Hε emissions of the active region observed during the 1958 eclipse are enhanced mainly by the increase of their source functions due to an increase in their excitation temperatures.

Key words: Chromosphere, Flash spectra, Spicules, Total solar eclipse.

1. Introduction

Physical parameters of the solar chromosphere are determined in two ways. One is the way that they can reproduce the solar UV spectrum. The other uses flash spectra of the total solar eclipse. Height distributions of the total hydrogen density and of the electron times proton density are shown in figure 1b and d. The thin curve distributions are the latest result from fitting the UV spectrum (Fontenla et al. 1993). In this determination the hydrostatic assumption confines the vertical extension and the chromosphere extends to around a height of 1800 km by the usual lifting forces of pressure and turbulence against gravity. In the second case the hydrostatic assumption is not necessary because the flash spectrum is a "side view" of the chromosphere. The thick curve distributions extending to the higher levels in figure 1b and d are the results of this study which will explain the emission lines visible in the flash spectrum of these levels.

The analysis made here is rather coarse and uses two simplifications: 1) The emission gradients of the eclipse curves reflect the density gradient and 2) Each analyzed emission line has its own constant excitation temperature, i.e., constant source function and ionization temperature throughout the chromosphere. In the low density chromosphere the relative populations among the atomic levels are mainly governed by radiative processes which have far longer scale heights than the density. This makes the excitation and ionization temperatures of each emission line change less against height and the chromospheric emission gradient equal to the density gradient. Zirker (1958) shows this in the case of metallic lines. In the higher density atmosphere collisions become more effective and change the populations of the atomic levels, which may decrease the temperature scale heights. The emission gradients will thus deviate from the density gradient.

Section 1 gives the derivation of the above distributions from emission gradients of metallic and Balmer lines in the high chromosphere, which extend the low chromosphere model (Hiei 1963) obtained with the continuous spectrum. The derived model reveals the spicule structure in the high chromosphere. Section 2 is an application of the model to Ca II H and K, and Hε line profiles obtained during the 1958 total solar eclipse (Suemoto and Hiei 1959, 1962). The same analysis is made for Balmer and Sr II lines using 1962 eclipse data (Dunn et al. 1968) in section 3. Section 4 studies 24 Ca II H and K spicules observed during the 1958 eclipse. Attached appendices give line profile data of Ca II H and K, and Hε observed during the 1958 eclipse and other information necessary for the text.

The reference coordinate system for the flash spectrum data used in this paper is depicted in figure 2 (ref. Thomas and Athay 1961). The whole area outside the moon's limb contributes to the emission in the slitless flash spectrum.

Numerical constants in the text are described in cgs-units.

2. Model of the Chromosphere

An empirical model of the low chromosphere has been obtained by Hiei (1963) with the use of a continuous spectrum of the 1958 total solar eclipse. The higher chromosphere, where many emission lines are visible during the eclipse, may be studied using their emission gradients. These are measured where the emission lines are weak and are closely related to the gradient of the emitting atom density, $n(h)$. Let $\beta'(h)$ be the density gradient of the emitting atom, then

$$\beta'(h) = -\frac{d \ln n(h)}{dh} \tag{1}$$

By integration

$$n(h) = n(0) \exp\left[-\int_0^h \beta'(h) dh\right] \tag{2}$$

* Osaka-Gakuin Junior College, Kishibe-Minami, Suita, Osaka 564–8511.

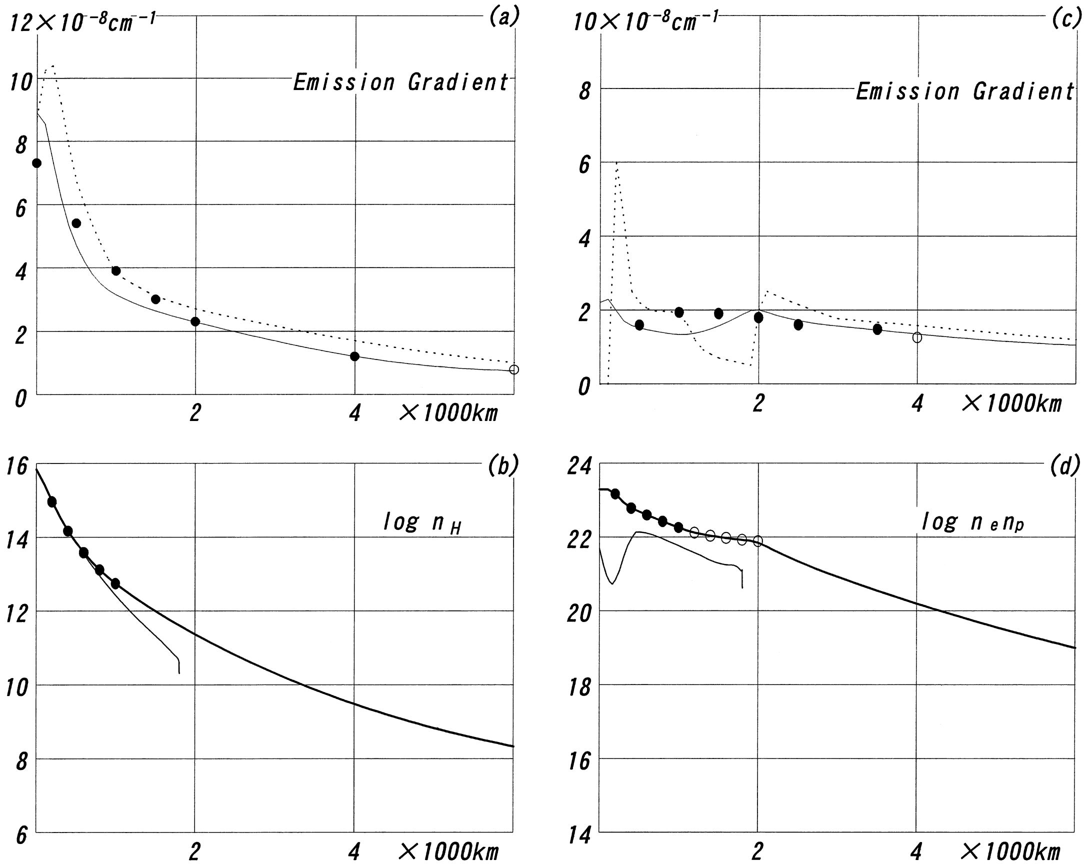

Fig. 1. Emission gradients and density distributions of the chromosphere. (a) Filled circles are emission gradients of the metallic lines compiled by Unsöld (1955). The open circle is obtained from the Ca II H and K lines observed during the 1958 eclipse. The solid curve is the emission gradient calculated from the dotted curve (the density gradient of hydrogen). (b) Filled circles are the densities of hydrogen from Hiei (1963). The thick curve is the hydrogen density distribution determined in this work. The thin curve is from the FAL-C model (Fontenla et al. 1993). (c) Filled circles are the emission gradients of the Balmer lines from the 1962 eclipse. The open circle is obtained from Hε during the 1958 eclipse. The solid curve is the emission gradient calculated from the dotted curve (the gradient of $n_e n_p$ distribution). (d) Filled and open circles show the $n_e n_p$ distribution from Hiei's work (Hiei 1963). The open circles are the values from the assumption, $n_e = n_p$. The thick curve is the $n_e n_p$ distribution determined in this work. The thin curve is from the FAL-C model (Fontenla et al. 1993). The height of the FAL-C model is shifted down by 400 km to reduce to the one used here, the origin of which is at the base of the chromosphere.

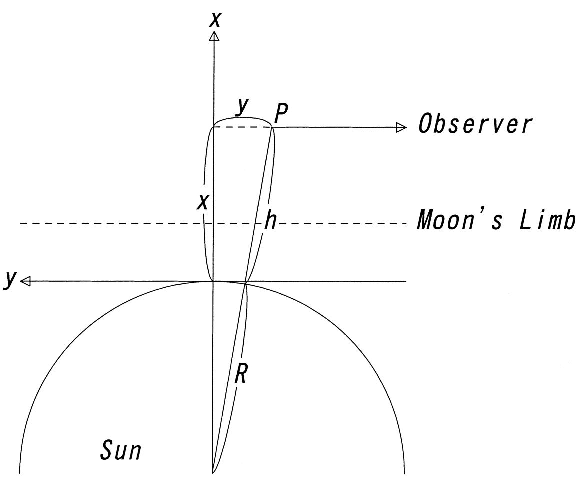

Fig. 2. The coordinate system (x, y) for the flash spectrum data. R: Sun's radius, h: height of an emitting atom at P from the base of the chromosphere. All the emitting atoms outside the moon's limb contribute to the emission of the slitless flash spectrum.

where $n(0)$ is the density at the base of the chromosphere, which is defined by the visible sun's limb. The number of the emitting atoms in the line of sight, $N(x)$, at the projected distance from the sun's limb, x, is

$$N(x) = \int_{-\infty}^{\infty} n(h)dy \tag{3}$$

where

$$h = x + \frac{y^2}{2R} \quad h \ll R \tag{4}$$

The total number, $N'(x)$, contributing to the intensity is

$$N'(x) = \int_{x}^{\infty} N(x)dx \tag{5}$$

Therefore, the emission gradient, $\beta(x)$, determined from weak emissions, should be

$$\beta(x) = -\frac{d \ln N'(x)}{dx} \tag{6}$$

If an approximation, $\beta'(h = x + \textit{emission scale height}) \sim \beta(x)$ (e.g., van de Hulst 1953), is applied, equation (6) can be calculated with the use of equations (1)–(5). The resultant $\beta(x)$ is compared with the observed one, and, by iteration, the final $n(h)$ is obtained from equation (2).

According to the study by Zirker (1958), the emission gradient of the metallic lines is equal to the total hydrogen density gradient. If in equation (1) n is replaced with the total hydrogen density, n_H, equation (6) provides the emission gradient of the metallic lines. The compiled values by Unsöld (1955) are adopted as the observed emission gradients. The gradient at $x = 6{,}000$ km is added from the Ca II H and K eclipse curves derived from 1958 eclipse data (see figures 4a and b, ref. appendix 1). Zirker's density gradients are the emission gradients asigned to special higher heights where the emission has the intensity of the "plate limit" (Zirker 1958) and were not used. The final iteration is shown in figure 1a. The discrepancy between the observed and calculated distribution is seen below 2,000 km, where the emission gradient of the metallic lines may not be equal to the density gradient. Hiei's hydrogen density is adopted below 1,000 km.

Balmer line intensities are proportional to the number of emitting atoms when the atmosphere is thin. Let n_j be the number density of the j-th level of hydrogen. Then by the Saha-Boltzmann equation it is

$$n_j = j^2 (n_e n_p) T^{-3/2} \exp\left[\frac{\chi_{ion} - \chi_j}{kT}\right] \Big/ C_1 \qquad (7)$$

where

$C_1 = (2\pi mk)^{3/2}/h^3 = 2.4147 \times 10^{15}$,
k : Boltzmann constant,
n_e : electron density,
n_p : proton density,
T : temperature,
X_j : excitation potential of the j-th level,
X_{ion} : ionization potential of hydrogen.

This equation shows that the gradient of the Balmer line intensity is equal to that of the cross product, $n_e n_p$, as long as the temperature gradient is negligible. This will occur in the high chromosphere where the density is low and the radiation is dominant, and equations (1)–(6) are applicable when $n(h)$ is replaced with $n_e n_p(h)$. The $\beta(x)$ are derived from Balmer line intensities from 1962 eclipse data (Dunn et al. 1968, see appendix 3). The gradient at $x = 4{,}000$ km is added from the $H\varepsilon$ eclipse curves derived from 1958 eclipse data (see figure 4c, ref. appendix 1). The result is shown in figure 1c and d. The discrepancy between observed and calculated distributions is seen in figure 1c below around 2,000 km and is probably due to an improper assumption. Hiei's $n_e n_p$ distribution is adopted below 2,000 km.

The n_H and $n_e n_p$ distributions in figure 1 give the ratio

$$n_e n_p / n_H = n_e x_H \qquad (8)$$

where x_H is the ionization degree of hydrogen. Since $x_H \leqq 1$, the ratio (8) gives the minimum of n_e. At $h = 5{,}000$ km, $\log n_H = 8.83$ and $\log(n_e n_p/n_H) = 10.73$. This means the minimum n_e exceeds n_H by a hundred times even although it is the main source of the electrons . A spicule structure can solve this contradiction. If the filling factor of the spicule has spherical symmetry, the derived values in figure 1 are taken as the ones of the spicule reduced by the filling factor. This solution is probable because a metallic line of Ca II H and a hydrogen line of $H\varepsilon$ in the 1958 eclipse data are well correlated (see appendix 2) and they may be emitted from the same volume. By assuming a spicule structure, equation (8) is rewritten as

$$n_e n_p / n_H = n_{es} x_H \qquad (9)$$

where n_{es} is the electron density of the spicule and n_H, $n_e n_p$ are taken as reduced or smoothed densities. In order to obtain the parameters of the spicule structure the following two assumptions are made:

1) $x_H = 1$ above $h = 4{,}200$ km. At this height $\log n_{es}$ becomes ~ 10.73 and equal to the hydrogen density, n_{Hs}, of the spicule, since the main electron source is hydrogen. n_{Hs} thus obtained is close to a recent theoretical value, $\log n_{Hs} = 10.6$ at $h = 4{,}000$ km, obtained by Kudoh and Shibata (1999). An higher n_{Hs} with a lower x_H leads to the denser atmosphere.

2) $n_{es} = n_e$ below $h = 2{,}000$ km. This is equivalent to $f = 1$. However, the separate determination of n_H from that of $n_e n_p$ causes a slight inconsistency around $h = 2{,}000$ km as shown in table 1 and figure 3. This assumption is reasonable since the hydrostatic chromosphere can extend to around $h = 2{,}000$ km.

With the above two assumptions the spicule electron density is drawn by hand between $h = 2{,}000$ km and 4,200 km. Once n_{es} is fixed, x_H is obtained from equation (9). On the other hand n_{Hs} is calculated for $h > 2{,}000$ km by the following formula,

$$\log n_{Hs} = \log n_{es} - \log x_H \qquad (10)$$

under the assumption that the main source of the electrons is hydrogen. Comparison of n_{Hs} with n_H gives the filling factor,

$$\log f = \log n_H - \log n_{Hs} \qquad (11)$$

The chromospheric model with the spicules is given in figure 3 and table 1.

3. Ca II H and K, and Hε Line Profiles during the 1958 Total Solar Eclipse

Unlike other slitless spectrum, the flash spectrum obtained during the 1958 eclipse (Suemoto and Hiei 1959, 1962)

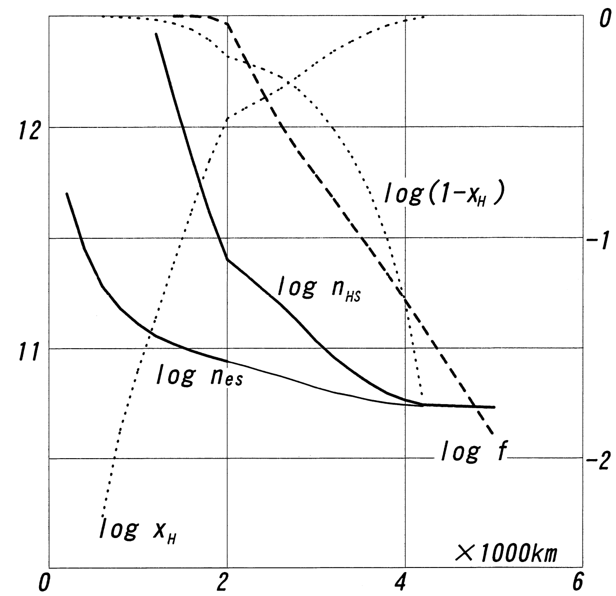

Fig. 3. Chromospheric model with spicules. n_{Hs}: hydrogen density and nes : electron density of the spicule, respectively, read by the left scale. x_H: ionization degree of hydrogen and f: filling factor of the spicule, read by the right scale. Thin part of the n_{es} curve is drawn by hand (see the text).

Table 1. Chromosphere Model.

height x1000km	Logn_H	Log$n_e n_p$	Log($n_e n_p$ / n_H)	Logn_{es}	Logx_H	Log($1-x_H$)	Logn_{Hs}	Log f
5.0	8.829	19.555	10.726				10.73	−1.901
4.8	8.946	19.676	10.730					
4.6	9.069	19.800	10.731					
4.4	9.199	19.929	10730					
4.2	9.335	20.060	10.725	10.733	−0.008	−1.739	10.741	−1.406
4.0	9.479	20.196	10.717	10.740	−0.023	−1.288	10.763	−1.284
3.8	9.630	20.334	10.704	10.749	−0.045	−1.007	10.794	−1.164
3.6	9.789	20.476	10.687	10.763	−0.076	−0.794	10.839	−1.050
3.4	9.955	20.621	10.666	10.781	−0.115	−0.633	10.896	−0.941
3.2	10.130	20.769	10.639	10.798	−0.159	−0.513	10.957	−0.827
3.0	10.313	20.920	10.607	10.820	−0.213	−0.412	11.033	−0.720
2.8	10.505	21.079	10.574	10.846	−0.272	−0.332	11.118	−0.613
2.6	10.706	21.251	10.545	10.871	−0.326	−0.277	11.197	−0.491
2.4	10.916	21.437	10.521	10.893	−0.372	−0.240	11.265	−0.349
2.2	11.135	21.638	10.503	10.918	−0.415	−0.211	11.333	−0.198
2.0	11.364	21.842	10.478	10.940	−0.462	−0.184	11.402	−0.038
1.8	11.605	21.919	10.314	10.963	−0.649	−0.110	11.612	−0.007
1.6	11.860	21.971	10.111	10.987	−0.876	−0.062	11.863	−0.003
1.4	12.130	22.033	9.903	11.018	−1.115	−0.035	12.133	−0.003
1.2	12.423	22.116	9.693	11.055	−1.362	−0.019	12.417	0.006
1.0	12.740	22.252	9.512	11.110	−1.598	−0.011		
0.8	13.110	22.420	9.310	11.180	−1.870	−0.006		
0.6	13.575	22.592	9.017	11.280	−2.263	−0.002		
0.4	14.165	22.785	8.620	11.450	−2.830			
0.2	14.960	23.160	8.200	11.700	−3.500			
0.0	15.836	(23.290)	(7.454)					

is one of a few which can provide line profiles. The peak intensity, E_0, total intensity, E, and $1/e$-line width, $\Delta\lambda_{1/e}$, of the Ca II H and K, and $H\varepsilon$ profiles have been measured (see appendix 1) in active and less active regions. They will be related to the chromospheric model in the previous section by the equations below.

Under the assumption of constant source function, S, the intensity at the projected height x and the wavelength distance from the line center $\Delta\lambda$ is

$$I(x, \Delta\lambda) = S[1 - \exp(-\tau(\Delta\lambda))] \tag{12}$$

τ is the optical thickness in the line of sight and given by

$$\tau(\Delta\lambda) = C_2 \lambda f_{abs} \int_{-\infty}^{\infty} \frac{n(h)}{V_D(h)} H(a, v) dy \tag{13}$$

where

$C_2 = \sqrt{\pi} e^2/(mc) = 1.4977 \times 10^{-2}$,
λ : wavelength of the line,
f_{abs} : absorption transition probability of the line,
$n(h)$: number density of the absorbing atom,
V_D : Doppler width in velocity scale,
$H(a, v)$: Voigt function with damping parameter a and $v = \Delta\lambda / V_D$.

The Doppler width taken from Suemoto's result (see figure 4, Suemoto 1963) is

$$V_D(\text{km/s}) = \begin{cases} 1.7 + 0.0051\, h & h < 3{,}580\,\text{km} \\ 19.959 & h \geq 3{,}580\,\text{km} \end{cases} \tag{14}$$

The measured quantities are

$$E_0(x) = \int_x^{\infty} I(x, 0) dx \tag{15}$$

$$E(x) = \int_{-\infty}^{\infty} d(\Delta\lambda) \int_x^{\infty} I(x, \Delta\lambda) dx \tag{16}$$

and $\Delta\lambda_{1/e}$ is obtained from

$$E_0(x) = e \int_x^{\infty} I(x, \Delta\lambda_{1/e}) dx \tag{17}$$

The number density in the ground level of Ca II is

$$n(h) = A_{\text{Ca}} n_H(h)(1 - x_{\text{Ca II}}) \tag{18}$$

where the calcium abundance relative to hydrogen, A_{Ca}, is -5.65 in logarithms, $n_H(h)$ is from table 1 and the ionization degree of the Ca II atom, $x_{\text{Ca II}}$, is

$$x_{\text{Ca II}} = \left[1 + n_{es} T_{\text{Ca II}}^{-3/2} \exp\left(\frac{\chi_{\text{Ca II}}}{k T_{\text{Ca II}}} \right) \Big/ C_1 \right]^{-1} \tag{19}$$

from the Saha equation. The electron density in equation (19) is the spicule's value in table 1, $T_{\text{Ca II}}$ is the ionization temperature of Ca II and $\chi_{\text{Ca II}} = 11.871\,\text{eV}$ is the ionization potential of Ca II. The fitting parameters to the observed Ca II H and K lines are the source function, $\mathcal{S}$, the ionization temperature, $T_{\text{Ca II}}$, and the damping parameter, a, in equations (12)–(19). The other constant parameters are $f_{abs}(\text{Ca II K}) = 0.682$, $f_{abs}(\text{Ca II H}) = 0.331$, $\lambda(\text{Ca II K}) = 3{,}934\,\text{A}$, and $\lambda(\text{Ca II H}) = 3{,}968\,\text{A}$. The result is shown in figures 4a and b. $\mathcal{S}$ is equivalent to the excitation temperature, T_{ex}, of 4,300 K and $T_{\text{Ca II}} = 6{,}000\,\text{K}$ in the less active region. In the active region only an increase of the excitation temperature to 4,690 K seems to be enough. Here, ionization of Ca II is necessary, otherwise it leads to a stronger intensity at greater heights and a broader width at lower heights. $a = 0.001$ can explain the intensity and width increases near $x = 0$.

The number density in the second level of hydrogen is

$$n(h) = 4[n_e n_p](h) T_{\text{BaC}}^{-3/2} \exp\left[\frac{\chi_{ion} - \chi_2}{k T_{\text{BaC}}} \right] \Big/ C_1 \tag{20}$$

(see equation (7)), where $[n_e n_p](h)$ is given by table 1 and

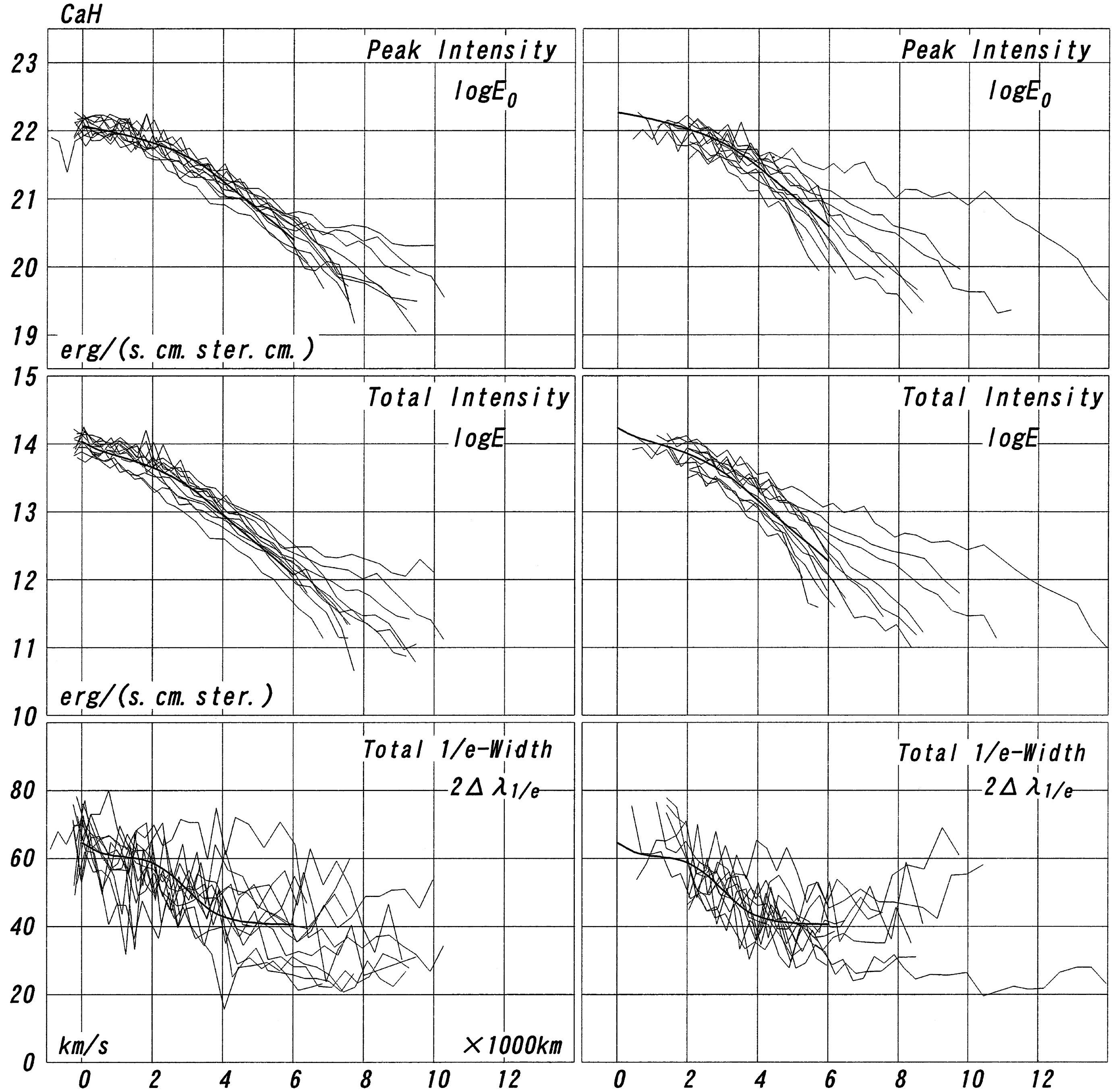

Fig. 4a. Fitting of the calculated curves (thick) to the observed Ca II H eclipse curves (thin).

$T_{\rm BaC}$ is the ionization temperature from the second level. The Doppler width should take into account the thermal broadening of hydrogen and equation (14) thus changes to

$$V_D = \sqrt{\frac{2kT_{\rm BaC}}{m_H} + [\text{equation(14)}]^2} \qquad (21)$$

where m_H is the hydrogen mass and the kinetic temperature is assumed to be $T_{\rm BaC}$. The other constant parameters are $f_{abs} = 0.0127$, $\lambda(H\varepsilon) = 3{,}970\,$A, $\chi_{ion} = 13.595\,$eV, $\chi_2 = 10.20\,$eV. Fitting to the observation of $H\varepsilon$ is made with the use of equations (12)–(17), (20) and (21). Figure 4c is the result with $T_{ex} = 4{,}520\,$K, $T_{\rm BaC} = 5{,}200\,$K and $a = 0$ for the less active region. For the active region only an increase of the excitation temperature to 5,110 K is sufficient.

4. Balmer and Sr II Emissions during the 1962 Eclipse

The chromospheric model in section 2 is applied to the total intensity of Balmer lines and Ca II-like Sr II resonance lines observed during the 1962 eclipse (Dunn et al. 1968).

Hα, Hβ, Hγ, Hε, H10, H15, and H20 are calculated with the use of the scheme for $H\varepsilon$ in section 3 but changing the wavelengths and transition probabilities (ref. Allen 1973). The result is shown in figure 5, with predictions of the peak intensities and $1/e$ widths. The fitting parameters are $a = 0$, $T_{\rm BaC} = 5{,}200\,$K, the same as for the 1958 eclipse, and excitation temperatures of 5,020 K, 4,860 K, 4,740 K, 4,720 K, 4,800 K, 4,840 K, 4,790 K for the above Balmer lines, respectively. Let b_j be NLTE factors and T_e the electron temperature, the relations

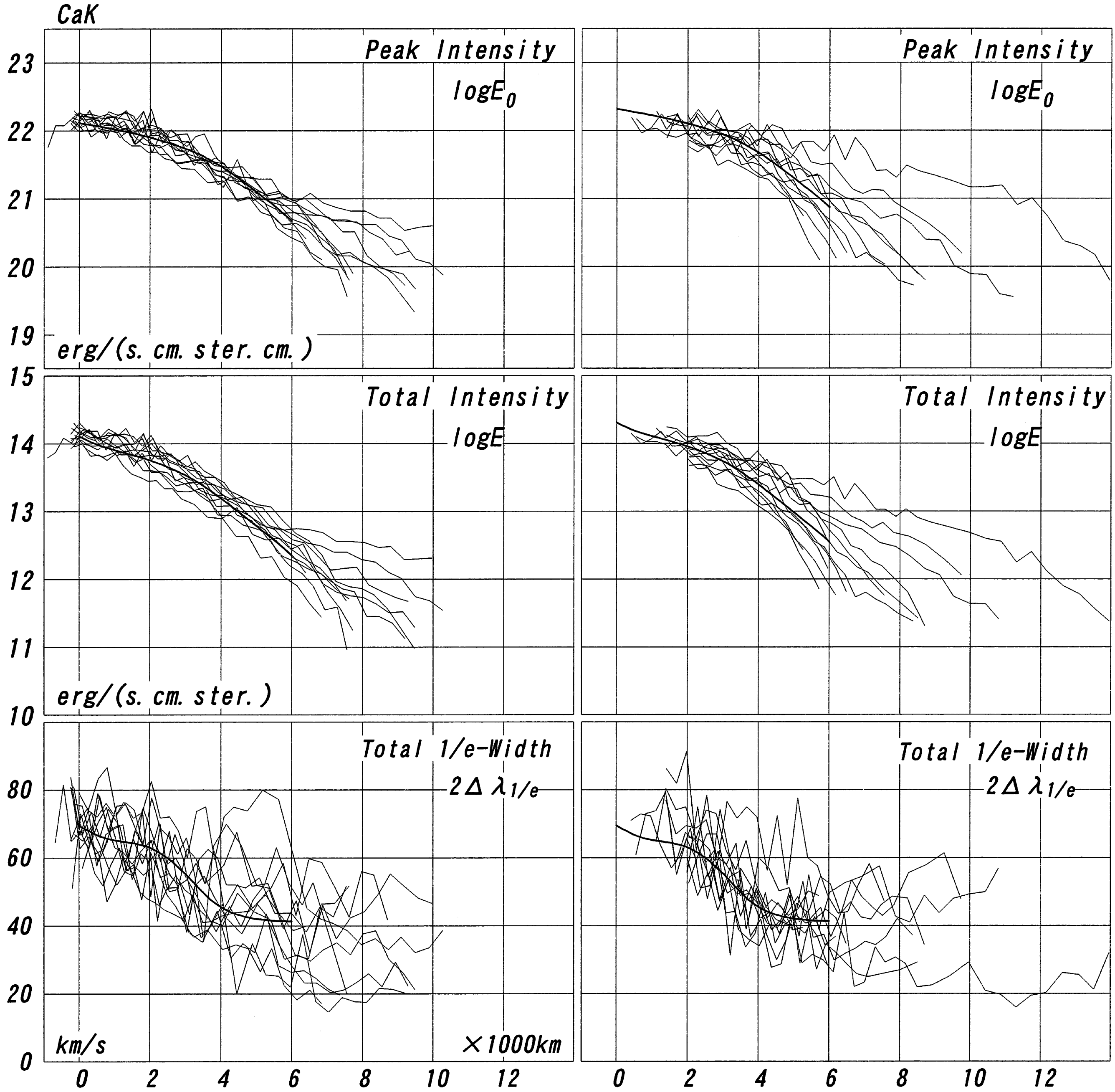

Fig. 4b. Fitting of the calculated curves (thick) to the observed Ca II K eclipse curves (thin).

$$T_{\mathrm{BaC}}^{-3/2} \exp\left(\frac{\chi_{\mathrm{ion}} - \chi_2}{kT_{\mathrm{BaC}}}\right) = b_2 T_e^{-3/2} \exp\left(\frac{\chi_{\mathrm{ion}} - \chi_2}{kT_e}\right) \quad (22)$$

from the Saha equation and

$$\exp\left(\frac{\chi_2 - \chi_j}{kT_{ex,j}}\right) = \frac{b_j}{b_2} \exp\left(\frac{\chi_2 - \chi_j}{kT_e}\right) \quad (23)$$

from the Boltzmann formula are obtained (ref. Thomas and Athay 1961). $T_{ex,j}$ is the excitation temperature of the j-th Balmer line. If $b_{20} = 1$, the combination of the above relations gives $T_e = 7{,}900$ K, $b_2 = 24.8$, $b_3 = 5.1$, $b_4 = 2.4$, $b_5 = 1.5$, $b_7 = b_{10} = b_{15} = 1.1$. These values can be compared with those of the VAL-C model (see tables 12 and 17, Vernazza et al. 1981). The electron temperature is comparable with Matsuno and Hirayama's result derived from Balmer and metallic line widths obtained from 1966 eclipse data (Matsuno and Hirayama 1988).

Sr II 4078 and 4216 intensities are calculated with the use of the scheme for Ca II in section 3 but changing the wavelengths, transition probabilities, abundance ratio, and ionization potential. The constant parameters used are f_{abs} (Sr II 4078)=0.708, f_{abs} (Sr II 4216)=0.339, $\chi_{\mathrm{Sr\,II}}$ =11.03 eV, $\log A_{Sr} = -9.1$. The result is shown in figure 6, with predictions of the peak intensities and $1/e$ widths. The fitting parameters are the ionization temperature of 5,140 K, the excitation temperature of 4,500 K and $a = 0$.

The Ca II H and K lines observed during the 1962 eclipse can also be explained by the chromospheric model with a slightly higher excitation temperature (see appendix 1).

5. Ca II H and K Spicules observed during the 1958 Eclipse

The total and peak intensities of the Ca II H and K

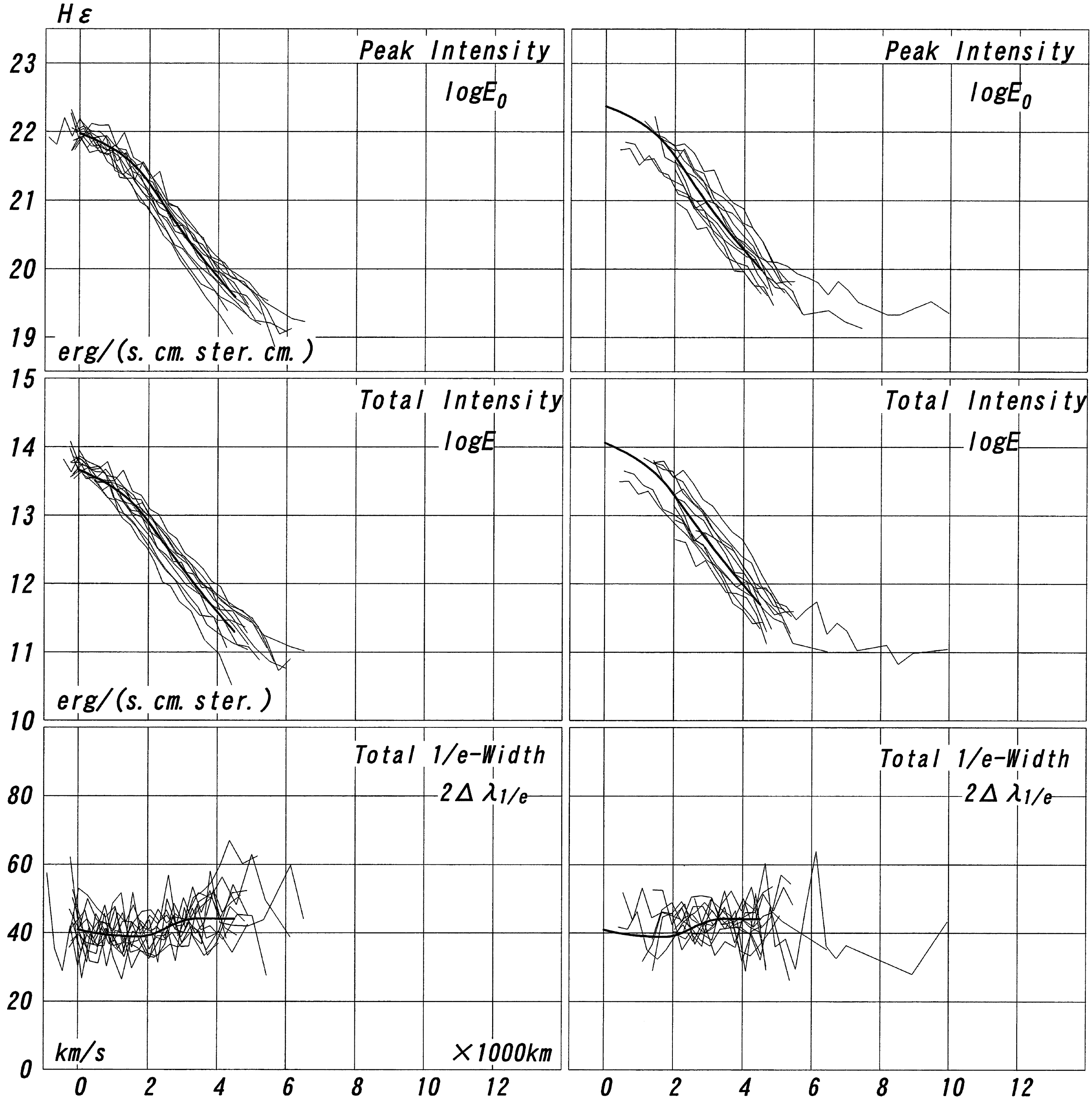

Fig. 4c. Fitting of the calculated curves (thick) to the observed Hε eclips curves (thin).

spicules have nearly the same emission gradients in the high chromosphere. Figure 7 shows the intensities overlapped by a shift on the Ca II K total intensity. Special attention is paid to the top height regions where the curves are linear. The spicules there are assumed not to be overlapped but isolated.

According to equation (13), in the thin atmosphere, the shifts give the intensity ratio of (Ca II K)/(Ca II H) as equal to 2 and the total to peak intensity ratio as equal to $\sqrt{\pi}V_D$, respectively. The emission gradients, intensity ratios and Doppler widths of the 24 spicules are listed in table 2. The averaged intensity ratio, (Ca II K)/(Ca II H), is less than 2 and might suggest thick spicules. However, Hirayama's examination (private communication, ref. Hirayama 1964) found that the color correction increased the Ca II K intensity relative to the Ca II H intensity by a small amount of 0.05 in logarithms and therefore the spicules are concluded to be thin.

Correlations between the top height, the total intensity at the top height, the emission gradient, and the Doppler width are shown in figure 8. Taller spicules have smaller emission gradients (a), spicules with brighter intensity at the top might be shorter (b) and have stronger turbulence (e). The other correlations are not remarkable. A difference between the active spicules and the less active ones is not obvious. However, their average total intensities at the top height (see table 2) are different by 0.2 in logarithms, which is equivalent to the excitation temperature difference obtained in section 3. The derived Doppler widths are compared with the measured $1/e$-widths in figure 9. The measured ones have a tendency to be narrower

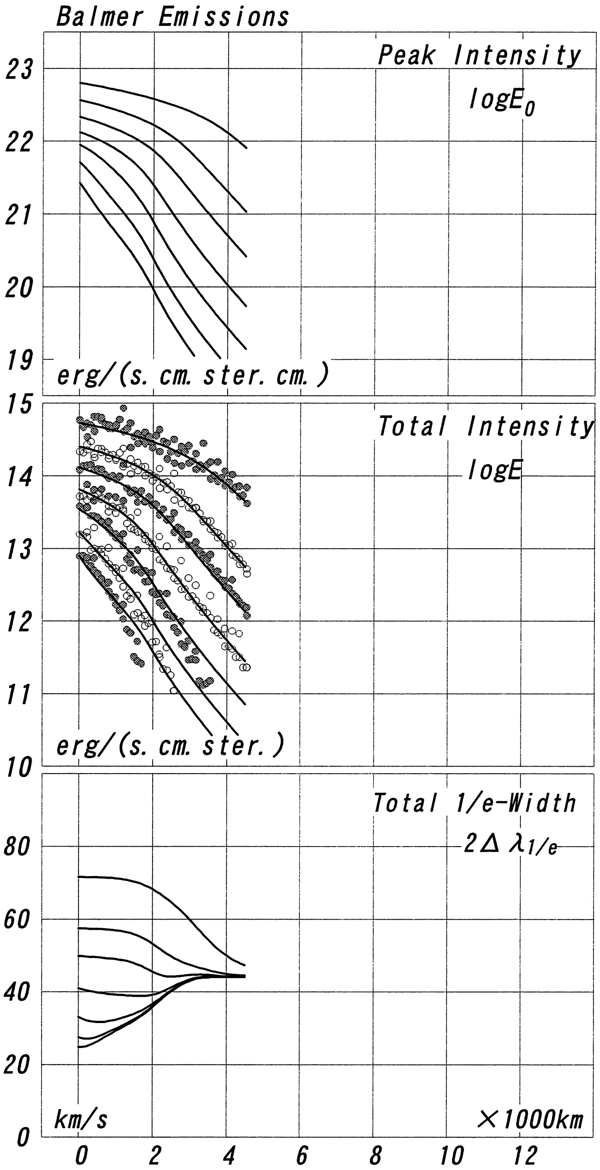

Fig. 5. Fitting of the calculated curves (solid) to the observed total intensities of the Balmer lines (circles). Each frame shows, from top to bottom, curves or circles for Hα, Hβ, Hγ, Hε, H10, H15, and H20.

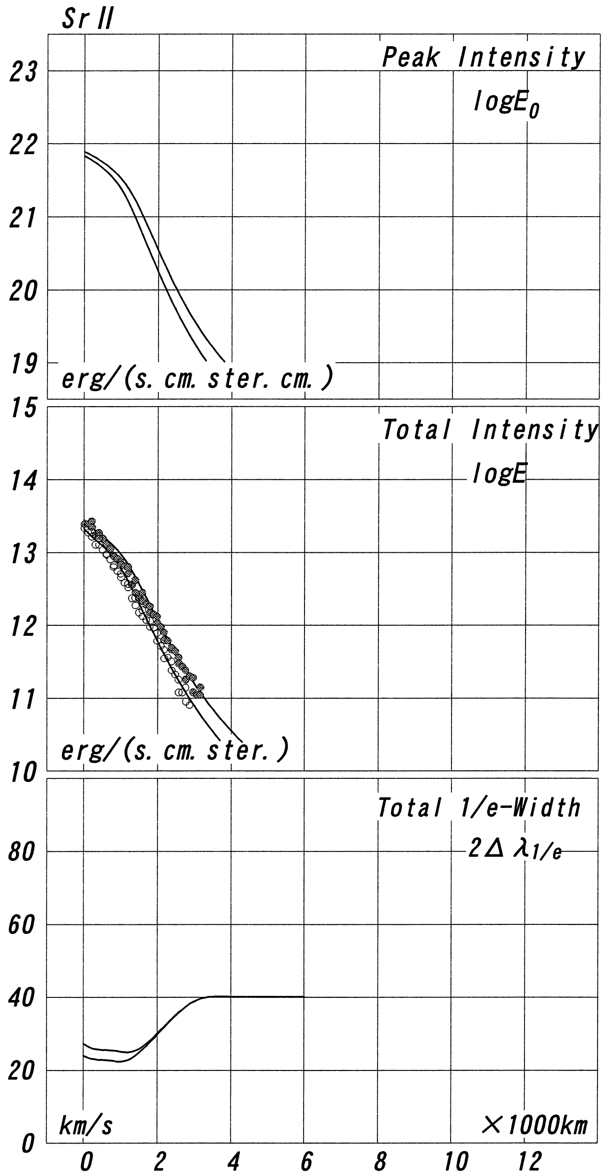

Fig. 6. Fitting of the calculated curves (solid) to the observed total intensities of Sr II 4078 and 4216 (circles). Each frame shows a curve or circles for Sr II 4078 upwards.

than the calculated ones. This may suggest that the line profile has a narrower core and broader wing than the Doppler profile does.

The total intensity of the spicules can give the intensity at the projection height x by the following formula (ref. equations (3) and (5)),

$$I(x) = \beta(x)E(x) \tag{24}$$

Since the spicules are thin,

$$I(x) = C_3 N_2 A_{21}/\lambda \tag{25}$$

where

$C_3 = hc/(4\pi) = 1.581 \times 10^{-17}$, $A_{21} = 1.5 \times 10^8$ is the spontaneous emission coefficient from the second level, and N_2 is the number in the line of sight of the second level of the Ca II atom. The number in the line of sight of the ground state is

$$N_1 = \frac{N_2}{2}\exp\left(\frac{\chi_2}{kT_{ex}}\right) \tag{26}$$

by the Boltzmann formula. The total number in the line of sight of hydrogen is calculated from equations (18) and (19), as

$$N_H(x) = \frac{N_1}{A_{\rm Ca}}\left[1 + C_1 T_{\rm Ca\,II}^{3/2}\exp\left(-\frac{\chi_{\rm Ca\,II}}{kT_{\rm Ca\,II}}\right)\Big/ n_{es}\right] \tag{27}$$

If the temperatures of the active and less active region obtained earlier are used, the total number of hydrogen can be calculated for reasonable electron densities. Furthermore, the geometrical thickness of the spicules will be estimated with $n_H \sim n_{es}$. In table 2 the thicknesses at the top are listed assuming $\log n_H = 10$ which is a little denser than the probable density of the corona. They are comparable with the "diameters" obtained by Nishikawa (1988). 14 spicules are thinner than 1,000 km and 19 thinner than 2,000 km. With an assumption of constant thickness along the height (Lynch et al. 1973; Nishikawa, private communication) , equation (27) gives the electron density at the bottom of the linear sections in figure 7. The bottom densities plotted in figure 10 are on the av-

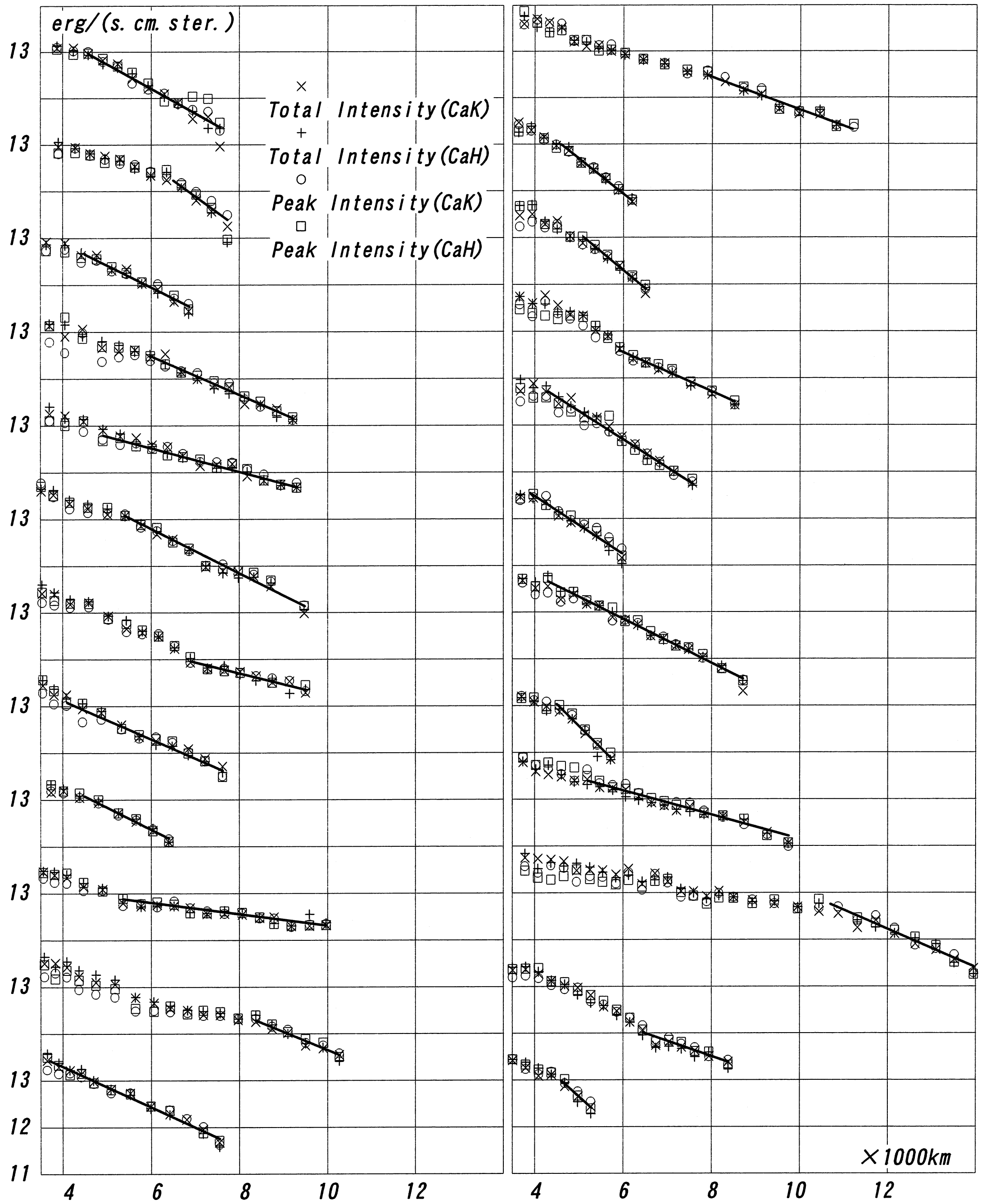

Fig. 7. Overlapped total and peak intensity eclipse curves of Ca II H and K spicules. Ordinates give the scale of the Ca II K total intensity. The solid lines give the emission gradients near the top of the spicules.

erage connected to the electron density of the mean spicule model in figure 3. This supports the assumption of the average top height density, $\log n_{es} = 10$. The large thickness of the short spicule no. 24 reduces to 870km if a revised top density, $\log n_{es} = 10.5$, is adopted. This still gives a reasonable bottom density of $\log n_{es} = 10.74$.

The electron density obtained from the red continuum of the 1970 eclipse data (Makita 1972) is plotted in figure 10. This assumed a thickness of 1 000 km. If this increases to 2,500 km, the plot moves on to the mean model.

6. Results and Discussion

1) Chromospheric structures

The spicules start around 2,000 km and have a filling factor of 0.05 at 4,000 km. Their starting height might be lowered (e.g., Suemoto and Hiei 1962; Kanno et al. 1971) if the spicule density near the top is increased to $\log n_{es} = 11$. The spicule model presented by Beckers (1968) has in the pertinent heights considerably high electron densities and fairly small filling factors.

The Ca II H and K profiles observed at lower projection heights than 2,500 km during the 1958 eclipse are not always symmetric and are classified into 3 groups: 28 percent with double equal intensity peaks, 14 percent with two unequal intensity peaks, and the rest with a single peak. This indicates that they are mainly shaped not by self absorption but by macroscopic motion. Suemoto (1963) reports a line shift of 19 km/s.

The optical thicknesses of Ca II K and Hε become thin at higher projection heights than 4,500 km and 2,000 km, respec-

Table 2. Ca II H and K Spicule Data.

No.	height range (km) bottom–top	gradient*	Log *Etop*	K/H ¥	K0/H0 ¥	K/K0 −8.5	H/H0 −8.5	Line Width (km/s)	Log *htop*	Log *N2top*	Log *N1top*	Thickness (km)	Log *N1bot.*	Log *n1bot.*	Log *nebot.*
1	4580−7560	1.227	11.37	0.2	0.2	0.25	0.25	24.1	3.46	7.68	11.07	684	12.66	4.82	10.88
2	6500−7730	1.577	11.39	0.25	0.2	0.1	0.05	16.1	3.59	7.81	11.20	920	12.04	4.08	10.44
3	4500−6860	1.089	11.54	0.25	0.3	0.0	−.05	12.8	3.58	7.80	11.19	897	12.31	4.35	10.60
4	5980−9220	0.951	11.15	0.25	0.4	−.1	0.05	13.0	3.13	7.35	10.74	319	12.08	4.57	10.72
5	4920−9300	0.583	11.68	0.25	0.25	0.05	0.05	15.2	3.45	7.57	10.96	527	12.07	4.35	10.59
6	5400−9480	1.094	11.14	0.275	0.25	0.325	0.325	28.7	3.18	7.40	10.79	359	12.73	5.17	11.09
7	6900−9500	0.537	11.35	0.3	0.3	0.15	0.15	19.1	3.08	7.30	10.69	286	11.30	3.84	10.33
8	4100−7620	0.952	11.62	0.25	0.35	0.2	0.3	24.3	3.60	7.82	11.21	942	12.67	4.69	10.80
9	4500−6400	1.096	12.17	0.3	0.3	0.25	0.25	24.1	4.21	8.43	11.82	3855	12.73	4.14	10.49
10	5360−9970	0.284	12.31	0.25	0.25	0.25	0.25	24.1	3.76	7.98	11.38	1377	11.94	3.81	10.30
11	8370−10280	0.897	11.54	0.3	0.2	0.2	0.15	20.3	3.49	7.71	11.11	740	11.85	3.98	10.39
12	3700−7550	0.998	11.76	0.25	0.25	0.25	0.25	24.1	3.76	7.98	11.37	1364	13.04	4.91	10.94
13	7900−11180	0.813	11.31	0.25	0.3	0.3	0.25	25.6	3.22	7.44	10.64	252	11.80	4.39	10.62
14	4600−6180	1.742	11.79	0.25	0.2	0.2	0.15	20.3	4.03	8.25	11.45	1629	12.64	4.43	10.64
15	5100−6500	1.820	11.90	0.2	0.25	0.2	0.25	22.8	4.16	8.38	11.58	2193	12.68	4.34	10.60
16	5900−8520	0.968	11.49	0.25	0.3	0.05	0.1	16.1	3.48	7.70	10.89	454	11.99	4.34	10.60
17	4300−7560	1.396	11.74	0.25	0.25	0.25	0.25	24.1	3.89	8.10	11.30	1164	13.28	5.21	11.14
18	3900−5970	1.442	12.25	0.2	0.15	0.3	0.25	25.6	4.41	8.63	11.83	3890	13.12	4.53	10.70
19	4300−8710	1.089	11.57	0.3	0.3	0.25	0.25	24.1	3.61	7.83	11.02	614	13.11	5.32	11.23
20	4500−5720	2.163	11.88	0.25	0.25	0.3	0.3	27.1	4.22	8.43	11.63	2489	12.78	4.38	10.62
21	5200−9750	0.598	12.21	0.25	0.25	0.3	0.35	28.7	3.99	8.21	11.40	1472	12.59	4.42	10.64
22	10700−13950	0.944	11.42	0.25	0.25	0.0	0.0	13.6	3.40	7.61	10.81	377	12.14	4.57	10.72
23	6440−8380	0.752	11.38	0.25	0.3	0.2	0.25	22.8	3.26	7.48	10.67	276	11.31	3.87	10.33
24	4600−5280	1.991	12.40	0.25	0.2	0.3	0.25	25.6	4.70	8.92	12.12	7586	12.70	3.82	10.30
	mean	1.125		0.253	0.260	0.191	0.195	21.8							

* multiply by 10^{-8} (cm^{-1})
\# in logarithms
¥ should be increased by 0.05 (see the text)

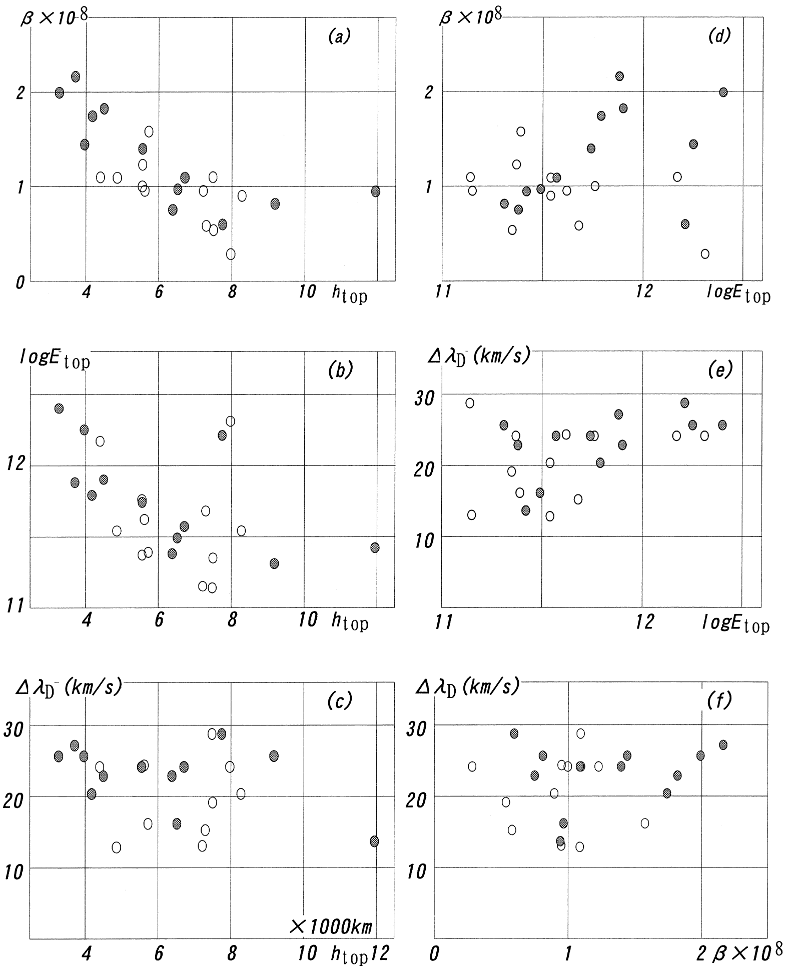

Fig. 8. Correlations of spicule parameters. The open and gray circles are from the less active and active regions, respectively. β: emission gradient, h_{top}: top height, E_{top}: total intensity at the top, and $\Delta\lambda_D$: Doppler width.

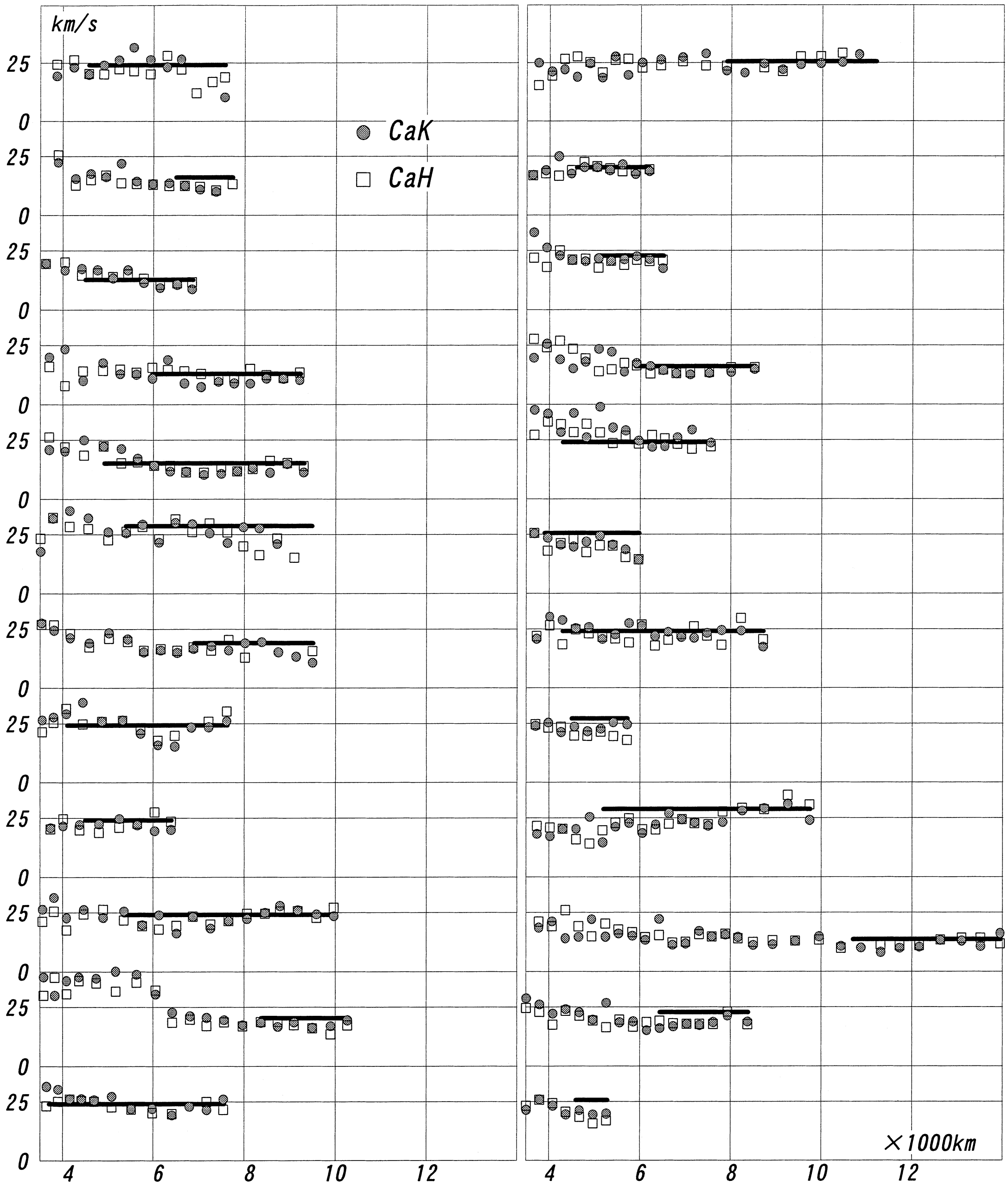

Fig. 9. Measured $1/e$ widths (symbols) and Doppler widths from the peak to total intensity ratio (solid lines).

tively, as shown in figure 11.

The radial or vertical optical thicknesses of Ca II K and Hα lines can be estimated from the spicule densities given in table 1. The dotted curves in figure 11 suggest that the Ca II K and Hα filtergrams see the chromosphere of $h = 4{,}000$–$5{,}000$ km.

2) Excitation and ionization.

Figure 12 shows a summary of the source functions obtained from this study, the brightness temperature curves, and the photospheric intensity from Allen (1973). The Hα emission and the Balmer continuum roughly correspond to half the photospheric intensity. The other emissions are weaker than this. The Ca II H and K, and Hε emissions from the active region are mainly enhanced by the increase of their source functions (gray circles, see section 3).

The ionization temperatures obtained are 6,000K for Ca II and 5,140 K for Sr II. They correspond to UV radiation of 5,450 K and 5,100 K, respectively (see figure 3, Vernazza et al. 1981). Ca II is half doubly ionized at $h = 1{,}100$ km, Sr II remains singly ionized below $h = 4{,}000$ km, in contrast with the half-ionized hydrogen at $h = 2{,}700$ km (see figure 3).

The excitation and ionization obtained should be explained by more detailed analysis.

3) Individual spicules

The individual spicules have a Doppler width of 22 km/s on the average and a typical top density of $\log n_{es} = 10$, which are consistent with theoretical predictions (e.g., Kudoh and Shibata, 1999). Their thicknesses are comparable with Nishikawa's (1988) and most of them are thinner than 2,000 km. The spicules of the active and less active region are similar in their physical parameters except that the active spicules have an higher excitation temperature (see section 5).

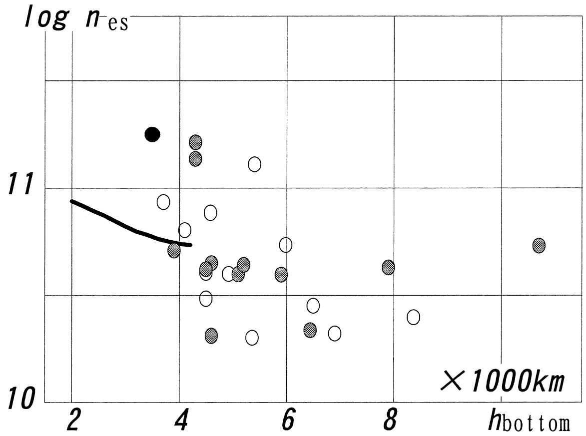

Fig. 10. Electron density of the spicules at their bottom heights (see the text). The open and gray circles are from the less active and active regions, respectively. The filled circle is from the 1970 eclipse (Makita 1972). The solid curve shows the average model in figure 3.

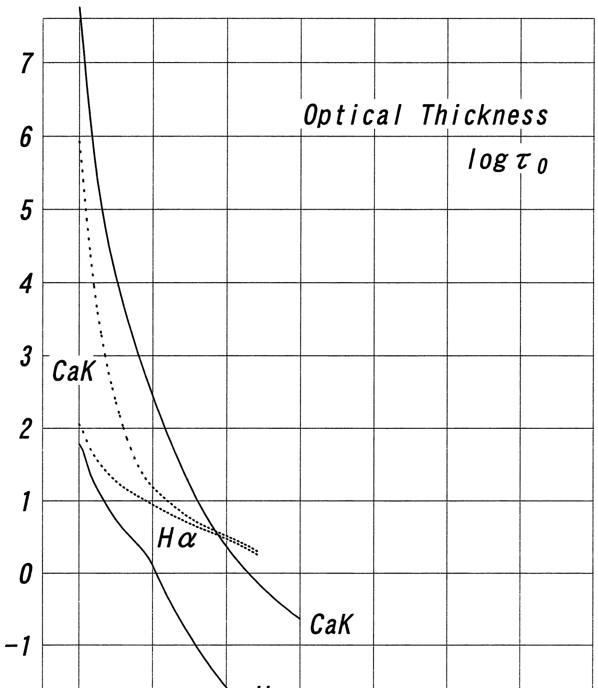

Fig. 11. Optical thickness of Ca II K, Hε, and Hα emission. The solid curves are for the flash spectrum. The dotted curves are radial or vertical optical thicknesses estimated from the spicule densities given in table 1.

The author expresses his hearty thanks to Professors Eijiro Hiei and Tadashi Hirayama for their encouragements. Thanks are also due to Professor Tadashi Hirayama for critical and valuable comments and to Dr. David Brooks for checking the manuscript.

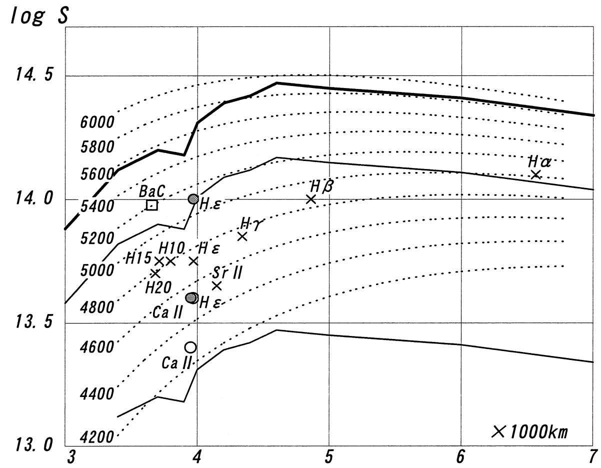

Fig. 12. Source functions of the emission lines. The open and gray circles are from the 1958 eclipse and for the less active and active regions, respectively. The crosses are from the 1962 eclipse. The square corresponds to the ionization temperature of the second level of hydrogen. The thick curve shows the photospheric brightness (Allen 1973). The thin curves are half and one tenth of the photospheric brightness. The dotted curves are brightnesses with the equivalent temperatures shown at their left ends.

Appendix 1. Ca II H and K, and Hε Emissions during the 1958 Total Solar Eclipse

The slitless flash spectrum of the 1958 total solar eclipse is rare in that it can provide line profiles (Suemoto and Hiei 1959, 1962). The peak intensity, total intensity, and $1/e$-width of Ca II H and K, and Hε profiles have been measured with a scanning slot equivalent to 5 km/s (wavelength resolution)$\times 0.65''$ (spatial resolution). 24 spicules were selected for the measurement and half of them (Nos. 13–24) were below an active corona. The identity of the spicules was lost below 4,000–5,000 km and the measured positions there relied on the scale of the microphotometer. The sun's visible limb, the base of the chromosphere, was determined from eclipse curves of the continuum. For the active region the determination was made by eye instead of scanning. This seems to produce a little more scatter in analyses of the active region data. The absolute calibration of the intensity was made by Hiei (1963). Hirayama later found a color sensitivity difference between Ca II K and Ca II H wavelength regions (private communication, ref. Hirayama 1964). The Ca II K intensity should be increased by 0.05 in logarithms relative to the Ca II H and Hε intensities. The listed intensities in the following tables do not take into account this correction. Table A1 gives the projected heights of the moon's limb at the measured positions, table A2a–c gives the Ca II H data, table A3a–c gives the Ca II K data, and table A4a–c gives the Hε data. A graphic presentation of these data was made earlier (Makita 2000). Figure A1 shows comparison of the total intensities obtained by other observers (Cillie and Menzel 1935; Houtgast 1957; Vjazanityn 1956; Dunn et al. 1968) with our average eclipse curves calculated in the text for the less-active region. The eclipse curves for the active region may pass through the data points of the other observers better.

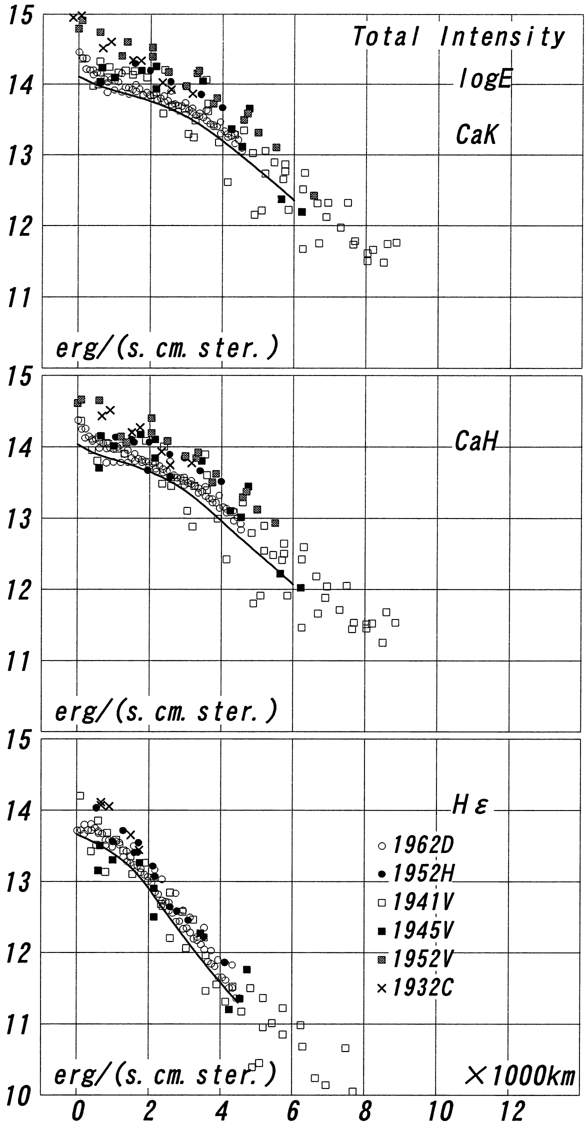

Fig. A1. Total intensities of Ca II H and K, and Hε. 1962D: Dunn et al. (1968), 1952H: Houtgast (1957), 1941V, 1945V and 1952V: Vjazanityn (1956), and 1932C: Cillie and Menzel (1935) are compared with the solid curves calculated in the text.

Appendix 2. Correlation between Ca II H and Hε Emissions

The Ca II H and H ε emissions tabulated in appendix 1 are combined in figure A2. They are close neighbors in the spectrum and measured by one and the same scanning. If different volumes of the chromosphere contribute to the emission, they may show separate behaviors. A good correlation of the two emissions in figure A2 is not contrary to the view that both the emissions are from the same volume. The slight dispersion seen in the active region diagram is due to the uncertainty of the height determination (see appendix 1).

Appendix 3. Emission Gradients of the Balmer Lines

Equation (7) in the text shows that the emission gradient of the Balmer lines is described by gradients of $n_e n_p$ and temperature. The latter gradient will be far smaller than the former in the high chromosphere where the density is low and the radiation is dominant. If this is the case, the emission gradient of the Balmer lines are related only to the gradient of $n_e n_p$. To increase the accuracy,

$$E_j \Bigg/ \left[C_3 (A_j/\lambda_j) C_1 j^2 T^{3/2} \exp\left(\frac{\chi_j - \chi_{\rm ion}}{kT} \right) \right]$$

are plotted against the projected height as in figure A3 and logarithmic gradients of $n_e n_p$ are obtained from the averaged curve. The Balmer lines, H4–H33, during the 1962 eclipse (Dunn et al. 1968), with log $E_j < 13.56$, are used. The constant parameters, A_j, λ_j, χ_j, are taken from Astrophysical Quantities by Allen (1973). The temperature is taken as 5,000 K which is effective only for low Balmer lines. The derived gradients are in table A5.

Reference

Allen, C. W. 1973, *Astrophysical Quantities*, The Athlone Press, Univ. London.

Beckers, J. M. 1968, *Solar Phys.*, **3**, 367.

Cillie, G. G. and Menzel, D. H. 1935, *Harvard College Obs. Circular*, 410.

Dunn, R. B., Evans, J. W., Jefferies, J. T., Orrall, F. Q., White, O. R., and Zirker, J. B. 1968, *Astrophys. J. Suppl.*, **15**, 275.

Fontenla, J. H., Avrett, E. H. and Loeser, R. 1993, *Astrophys. J.*, **406**, 319.

Hiei, E. 1963, *Publ. Astron. Soc. Japan*, **15**, 277.

Hirayama, T. 1964, *Publ. Astron. Soc. Japan*, **16**, 104.

Houtgast, J. 1957, *Rech. Astron. Obs. Utrecht*, **XIII**, 3.

Kanno, M., Tsubaki, T. and Kurokawa, H. 1971, *Solar Phys.*, **21**, 314.

Kudoh, T. and Shibata, K. 1999, *Astrophys. J.*, **514**, 493.

Lynch, D. K., Beckers, J. M. and Dunn, R. B. 1973, *Solar Phys.*, **30**, 63.

Makita, M. 1972, *Solar Phys.*, **24**, 59.

Makita, M. 2000, in *The Last Total Solar Eclipse of the Millenium in Turkey*, ASP Conference, vol. 205, p. 97.

Matsuno, K. and Hirayama, T. 1988, *Solar Phys.*, **117**, 21.

Nishikawa, T. 1988, *Publ. Astron. Soc. Japan*, **40**, 613.

Suemoto, Z. and Hiei, E. 1959, *Publ. Astron. Soc. Japan*, **11**, 122.

Suemoto, Z. and Hiei, E. 1962, *Publ. Astron. Soc. Japan*, **14**, 33.

Suemoto, Z. 1963, *Publ. Astron. Soc. Japan*, **15**, 531.

Thomas, R. N. and Athay, R. G. 1961, *Physics of the Solar Chromosphere*, Interscience Publ., New York.

Unsöld, A. 1955, *Physik d. Sternatmosphären*, II-ed., Springer.

Vernazza, J. E., Avrett, E. H. and Loeser, R. 1981, *Astrophys. J. Suppl.*, **45**, 635.

van de Hulst, H. C. 1953, The Chromospher and the Corona, in *The Sun*, ed. G. P. Kuiper, Univ. Chicago Press, p. 207.

Vjazanityn, V. P. 1956, *Report Main Astron. Obs. Pulkovo XX*, 3, p. 16.

Zirker, J. B. 1958, *Astrophys. J.*, **127**, 680.

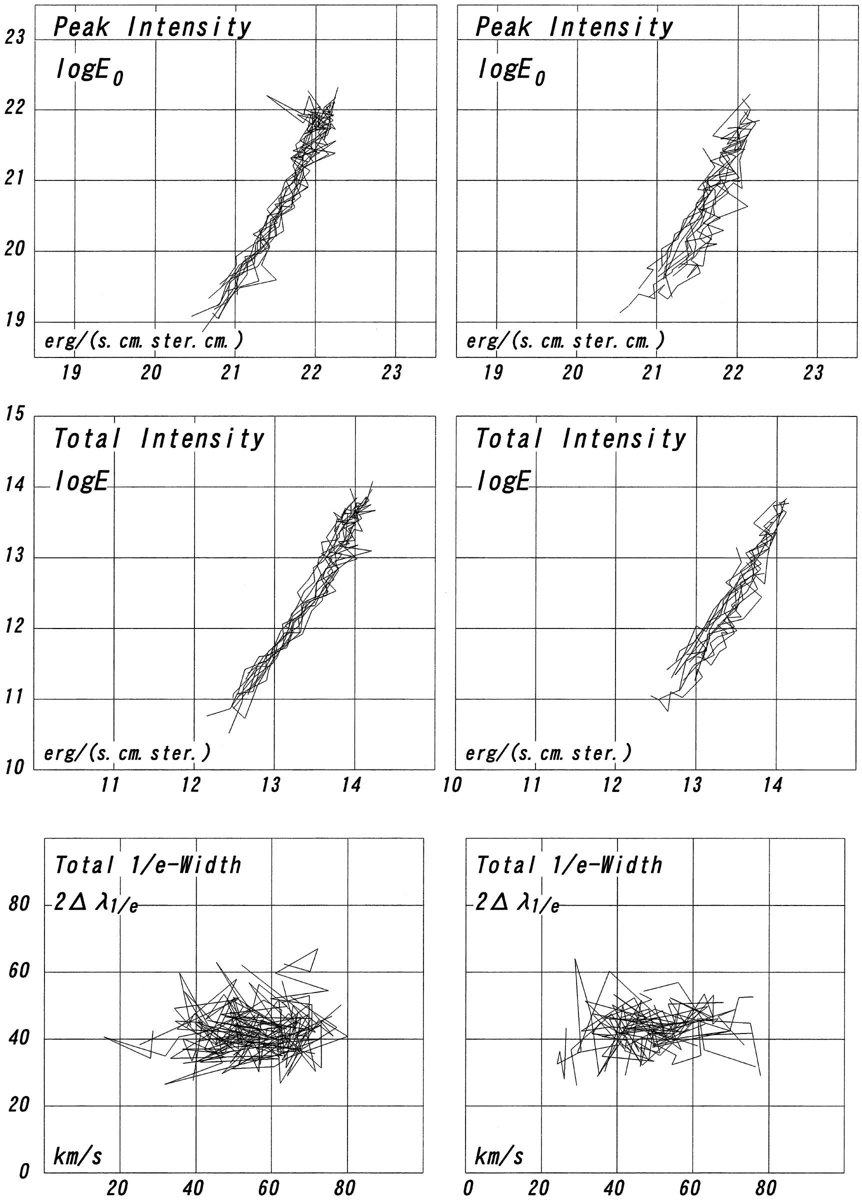

Fig. A2. Correlation between Ca II H (abscissa) and Hε(ordinate) emissions from the 1958 eclipse data.

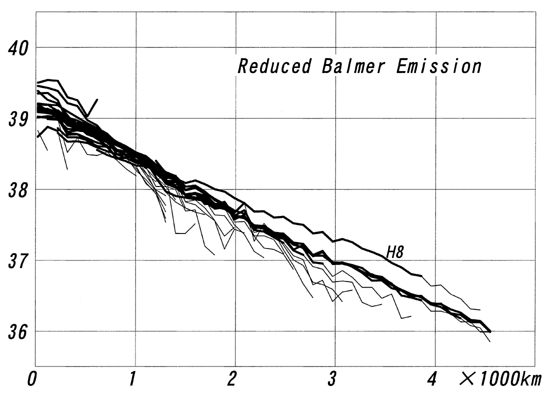

Fig. A3. Reduced Balmer line emissions to the integrated $n_e n_p$. H8 runs higher due to the blend with the He line. The part with the thin lines corresponds to the weaker intensity, $\log E < 11.8$, and they run lower, probably due to a calibration problem.

Table A1. Height of the Measured Position (km).

traced position no.	1	2	3	4	5	6	7	8	9	10	11	12	13	14	15	16	17	18	19	20	21	22	23	24	traced position no.
position angle*	48.7	48.0	47.5	45.0	44.7	44.0	43.6	42.1	42.7	41.5	40.9	40.0	33.4	32.8	31.9	31.6	31.3	31.0	29.5	30.3	28.9	27.9	27.3	27.5	position angle*
frame no.																									frame no.
71				9210	9300	9470	9500			9970	10270														71
70	7560	7730		8850	8940	9100	9140			9590	9900														70
69	7290	7370		8480	8560	8720	8750			9180	9500														69
68	6940	7020		8120	8180	8330	8380			8790	9100		11210									13950			68
67	6610	6685	6850	7770	7840	7980	8020			8460	8740		10810									13515			67
66	6300	6350	6520	7430	7490	7630	7660			8065	8370		10440									13100			66
65	5935	5990	6150	7050	7110	7240	7280	7620		7665	7970		9970									12630			65
64	5570	5630	5790	6680	6720	6860	6890	7220		7265	7565		9520									12165			64
63	5240	5290	5440	6320	6370	6490	6530	6840		6880	7180	7550	9120									11730			63
62	4910	4955	5110	5980	6020	6130	6170	6480	6400	6520	6820	7180	8710									11310			62
61	4575	4620	4770	5630	5660	5770	5800	6110	6040	6135	6430	6800	8290									10875			61
60	4240	4280	4420	5270	5300	5410	5440	5730	5660	5770	6060	6420	7890								9745	10440			60
59	3870	3900	4050	4890	4910	5010	5030	5330	5260	5360	5640	5990	7430			8520					9265	9960			59
58	3460	3485	3630	4450	4470	4570	4590	4875	4810	4900	5180	5525	6920			8000			8710		8740	9430			58
57	3080	3100	3240	4050	4050	4155	4170	4450	4380	4470	4750	5090	6440			7520	7560		8230		8260	8930	8380		57
56	2740	2760	2890	3700	3700	3790	3810	4080	4015	4090	4365	4700	6030	6190		7100	7140		7800		7830	8500	7940		56
55	2490	2500	2635	3440	3430	3515	3535	3800	3735	3810	4090	4420	5720	5890	6490	6790	6820		7480		7510	8170	7620		55
54	2265	2275	2405	3200	3190	3275	3290	3550	3490	3560	3830	4160	5440	5600	6200	6500	6540		7190		7210	7890	7320		54
53	2040	2050	2180	2965	2950	3035	3045	3300	3240	3310	3580	3905	5160	5325	5920	6220	6260		6910		6930	7595	7035		53
52	1820	1820	1950	2730	2710	2790	2800	3050	2990	3055	3320	3645	4885	5045	5640	5920	5970	5970	6620		6640	7310	6740		52
51	1590	1590	1715	2490	2465	2545	2555	2800	2740	2800	3060	3385	4605	4765	5355	5650	5680	5680	6330		6350	7010	6440		51
50	1365	1365	1485	2255	2225	2300	2310	2550	2500	2550	2815	3130	4330	4485	5080	5370	5400	5400	6045		6060	6720	6155		50
49	1140	1135	1255	2020	1985	2060	2065	2300	2250	2300	2560	2870	4050	4205	4795	5090	5120	5120	5760	5720	5770	6430	5860		49
48	910	900	1020	1775	1735	1805	1815	2040	1990	2035	2295	2600	3760	3920	4505	4800	4820	4820	5460	5420	5470	6125	5560		48
47	685	675	790	1540	1500	1565	1570	1790	1750	1790	2045	2350	3490	3640	4230	4520	4540	4540	5175	5140	5190	5840	5270	5270	47
46	460	440	555	1300	1255	1320	1325	1540	1500	1530	1790	2090	3205	3355	3940	4235	4260	4260	4880	4850	4900	5540	4975	4975	46
45	230	210	325	1065	1010	1070	1075	1285	1245	1280	1530	1830	2920	3075	3660	3950	3970	3970	4590	4560	4605	5250	4680	4680	45
44	0	−20	90	820	765	820	825	1030	995	1020	1270	1570	2640	2790	3370	3660	3680	3680	4300	4270	4310	4950	4380	4380	44
43	−220	−245	−145	590	530	580	585	785	750	770	1020	1315	2365	2520	3090	3380	3400	3400	4020	3990	4030	4660	4090	4090	43
42	−445			350	290	340	340	535	500	520	765	1060	2090	2235	2810	3100	3120	3120	3730	3705	3740	4370	3800	3800	42
41	−675			110	45	90	95	280	250	265	510	795	1805	1950	2530	2810	2830	2830	3440	3415	3445	4075	3505	3505	41
40	−900			−125	−195	−150	−155	30	0	10	255	540	1555	1675	2250	2530	2550	2550	3155	3130	3160	3785	3210	3210	40
39								−220	−250	−245	0	280	1250	1390	1960	2250	2260	2260	2860	2840	2865	3490	2915	2915	39
38											−250	25	970	1115	1680	1970	1980	1980	2580	2560	2580	3200	2630	2630	38
37												−235	695	835	1400	1680	1700	1700	2290	2270	2290	2910	2340	2340	37
36													415	555	1120	1400	1410	1410	2000	1990	2000	2620	2040	2040	36

*degree from the east end of the equator

Table A2a. Total Intensity (log E − 10) of Ca II H (erg/sec.cm.ser).

traced position no.	1	2	3	4	5	6	7	8	9	10	11	12	13	14	15	16	17	18	19	20	21	22	23	24	traced position no.
position angle*	48.7	48.0	47.5	45.0	44.7	44.0	43.6	42.1	42.7	41.5	40.9	40.0	33.4	32.8	31.9	31.6	31.3	31.0	29.5	30.3	28.9	27.9	27.3	27.5	position angle*
frame no.																									frame no.
71				0.877	1.422		1.059			2.115	1.123														71
70	1.144	0.661		0.928	1.465	0.791	0.969			2.302	1.409														70
69	1.150	1.289		1.192	1.597	1.358	1.266			2.050	1.494														69
68	1.519	1.630		1.349	1.764	1.484	1.243			2.103	1.700											1.007			68
67	1.664	1.826	1.137	1.432	1.855	1.471	1.378			2.234	1.890		1.132									1.250			67
66	1.827	2.159	1.432	1.541	1.843	1.569	1.563			2.301	2.095		1.477									1.651			66
65	2.066	2.070	1.577	1.753	1.974	1.736	1.517	1.336		2.376	2.014		1.466									1.774			65
64	2.327	2.234	1.782	1.882	2.067	2.061	1.726	1.569		2.322	2.141		1.543									1.882			64
63	2.456	2.403	2.012	2.072	2.154	2.271	1.950	1.703		2.341	2.176	1.335	1.780									2.010			63
62	2.535	2.456	2.102	2.271	2.310	2.471	2.191	1.896	1.799	2.482	2.204	1.621	1.880									2.160			62
61	2.736	2.556	2.324	2.332	2.376	2.632	2.305	1.925	2.089	2.489	2.300														61
60	2.819	2.671	2.433	2.468	2.574	2.789	2.540	2.101	2.294	2.466	2.384	2.018	2.234								1.797	2.514			60
59	2.930	2.805	2.601	2.552	2.679	2.948	2.632	2.319	2.425	2.629	2.483	2.155	2.307			1.185					2.008	2.440			59
58	3.111	2.899	2.614	2.663	2.890	3.042	2.943	2.641	2.668	2.867	2.853	2.446	2.468			1.449			1.225		2.312	2.568			58
57	3.171	3.120	2.859	2.905	2.906	3.137	2.982	2.810	2.784	2.969	2.965	2.569	2.553			1.578	1.453		1.553		2.375	2.547	0.997		57
56	3.210	3.102	2.998	2.926	3.154	3.350	3.134	2.936	2.938	3.151	3.055	2.757	2.666	1.590		1.867	1.752		1.739		2.417	2.654	1.342		56
55	3.361	3.336	3.080	3.016	3.208	3.376	3.302	3.127	3.028	3.209	3.244	2.993	2.769	1.767	1.725	1.965	1.919		1.900		2.472	2.685	1.242		55
54	3.442	3.358	3.134	3.043	3.244	3.463	3.355	3.310	3.136	3.230	3.134	2.975	2.808	1.985	1.923	2.069	2.019		2.009		2.521	2.623	1.417		54
53	3.546	3.283	3.282	3.192	3.427	3.600	3.398	3.298	3.175	3.368	3.346	3.135	2.944	2.220	2.130	2.192	2.266		2.099		2.620	2.744	1.464		53
52	3.628	3.419	3.372	3.232	3.502	3.594	3.653	3.357	3.224	3.440	3.330	3.326	2.984	2.358	2.347	2.412	2.416	1.831	2.195		2.671	2.832	1.437		52
51	3.769	3.536	3.499	3.337	3.612	3.699	3.639	3.482	3.358	3.766	3.502	3.343	3.228	2.687	2.563	2.665	2.630	2.111	2.415		2.728	3.081	1.702		51
50	3.735	3.553	3.482	3.510	3.742	3.794	3.724	3.594	3.502	3.603	3.525	3.341	3.175	2.736	2.751	2.843	2.916	2.424	2.528		2.795	3.020	1.981		50
49	3.770	3.632	3.607	3.520	3.659	3.755	3.625	3.668	3.519	3.636	3.687	3.396	3.267	2.877	2.797	3.085	3.023	2.596	2.702	1.591	2.942	2.987	2.130		49
48	3.867	3.801	3.724	3.579	3.837	4.207	4.040	3.788	3.799	4.026	3.990	3.666	3.507	3.131	2.980	3.167	3.155	2.746	2.830	1.657	3.012	3.123	2.339		48
47	3.917	3.742	3.644	3.530	3.750	3.806	3.870	3.670	3.650	3.792	3.671	3.579	3.340	3.001	3.146	3.163	3.350	2.938	2.882	2.217	3.060	3.069	2.396	2.027	47
46	3.814	3.776	3.737	3.615	3.874	3.934	3.990	3.724	3.784	3.998	3.805	3.712	3.493	3.295	3.500	3.330	3.582	3.095	3.131	2.461	3.117	3.186	2.571	2.280	46
45	3.910	3.821	3.825	3.582	3.848	3.850	4.093	3.885	3.930	3.917	3.806	3.581	3.538	3.343	3.481	3.338	3.547	3.227	3.142	2.675	3.270	3.296	2.793	2.694	45
44	4.024	3.881	3.731	3.785	3.997	4.093	4.008	3.993	3.881	4.010	4.011	3.967	3.766	3.526	3.615	3.493	3.718	3.308	3.477	2.639	3.475	3.375	2.878	2.869	44
43	3.857	3.825	3.801	3.748	3.841	3.965	4.048	3.769	3.908	3.992	4.045	3.936	3.696	3.364	3.550	3.546	3.678	3.497	3.345	2.851	3.391	3.318	3.064	3.002	43
42				3.829	3.838	3.989	4.026	3.955	3.856	4.082	4.000	4.043	3.804	3.729	3.776	3.810	3.910	3.767	3.415	2.918	3.560	3.391	3.172	3.128	42
41				3.948	4.255	4.200	4.175	3.969	3.887	3.987	3.986	3.939	3.661	3.720	3.756	3.652	3.805	3.615		3.115	3.433	3.265	3.160	3.190	41
40				3.947	3.920	3.984	4.150	4.017	4.048	4.129	4.094	4.087	3.904	3.694	3.950	3.914	3.941	3.883	3.690	3.216	3.630	3.585	3.347	3.320	40
39								4.062	3.937	4.218	4.210	4.130	3.993	3.915	4.119	4.021	4.070	3.861	3.728	3.447	3.741	3.814	3.479	3.451	39
38												4.140	3.780	3.836	4.074	4.029	4.024	3.945	3.775	3.407	3.851	3.599	3.495	3.497	38
37												4.082	3.947	3.992	4.044	3.955	4.100	3.713	3.858	3.560	3.886	3.689	3.571	3.678	37
36													3.913	4.080	4.125	4.152	4.024	3.986	3.930	3.497	3.936	3.846	3.606	3.623	36

*degree from the east end of the equator

Table A2b. Peak Intensity ($\log E_0 - 19$) of Ca II H (erg/sec.com.ster.cm).

traced position no.	1	2	3	4	5	6	7	8	9	10	11	12	13	14	15	16	17	18	19	20	21	22	23	24	traced position no.
position angle*	48.7	48.0	47.5	45.0	44.7	44.0	43.6	42.1	42.7	41.5	40.9	40.0	33.4	32.8	31.9	31.6	31.3	31.0	29.5	30.3	28.9	27.9	27.3	27.5	position angle*
frame no.																									frame no.
71				0.375	0.871		0.496			1.320	0.553														71
70	0.523	0.169		0.503	0.939	0.043				1.313	0.862														70
69	1.033	0.850		0.713	1.029	0.586	0.553			1.310	0.936														69
68	1.084	1.137		0.823	1.272	0.753				1.346	1.086		0.366									0.504			68
67	0.946	1.334	0.683	1.017	1.384	0.800	0.760			1.490	1.251		0.318									0.765			67
66	0.981	1.661	0.977	1.148	1.306	0.853	0.802			1.586	1.443		0.630									1.115			66
65	1.371	1.601	1.159	1.266	1.476	0.902	0.846	0.438		1.618	1.381		0.636									1.301			65
64	1.604	1.713	1.261	1.340	1.532	1.272	1.103	0.776		1.577	1.517		0.691									1.443			64
63	1.739	1.871	1.462	1.509	1.567	1.406	1.343	0.943		1.577	1.549	0.718	1.083									1.595			63
62	1.903	1.818	1.587	1.688	1.710	1.719	1.548	1.203	1.058	1.766	1.471	0.881	1.173									1.708			62
61	2.021	1.976	1.755	1.802	1.765	1.783	1.674	1.252	1.284	1.813	1.640														61
60	1.994	2.027	1.790	1.875	1.943	1.978	1.809	1.339	1.544	1.775	1.527	1.363	1.497								0.964	2.107			60
59	2.107	2.024	1.908	1.891	1.875	2.150	1.926	1.475	1.666	1.886	1.591	1.451	1.543			0.663					1.119	1.905			59
58	2.316	2.279	1.932	2.062	2.299	2.154	2.242	1.815	1.945	2.048	2.015	1.713	1.652			0.870			0.477		1.472	2.096			58
57	2.316	2.428	2.179	2.515	2.201	2.264	2.257	2.015	2.093	2.234	2.086	1.803	1.780			1.068	0.841		0.738		1.543	2.021	0.317		57
56	2.412	2.298	2.246	2.331	2.303	2.405	2.312	2.008	2.137	2.434	2.195	1.949	1.910	0.901		1.330	1.014		1.043		1.602	2.131	0.599		56
55	2.572	2.583	2.369	2.398	2.424	2.603	2.488	2.283	2.274	2.409	2.407	2.156	1.979	1.128	1.033	1.437	1.139		1.189		1.763	2.138	0.613		55
54	2.619	2.573	2.417	2.318	2.451	2.579	2.490	2.518	2.286	2.445	2.224	2.121	1.958	1.362	1.234	1.476	1.245		1.227		1.767	2.010	0.804		54
53	2.736	2.572	2.595	2.468	2.581	2.744	2.603	2.504	2.384	2.557	2.527	2.327	2.191	1.572	1.439	1.633	1.459		1.368		1.847	2.183	0.850		53
52	2.753	2.618	2.639	2.547	2.704	2.704	2.742	2.467	2.401	2.578	2.394	2.504	2.192	1.694	1.678	1.804	1.650	1.252	1.533		1.915	2.257	0.809		52
51	2.973	2.828	2.737	2.588	2.748	2.801	2.912	2.706	2.563	2.906	2.525	2.486	2.399	1.950	1.889	2.004	1.808	1.536	1.766		2.012	2.540	1.070		51
50	2.827	2.687	2.834	2.816	2.824	2.850	2.850	2.713	2.546	2.785	2.625	2.583	2.352	2.012	2.064	2.264	2.104	1.776	1.748		2.113	2.497	1.323		50
49	2.872	2.840	2.854	2.740	2.710	2.842	2.834	2.770	2.671	2.847	2.695	2.492	2.567	2.218	2.059	2.450	2.160	1.946	2.043	0.939	2.146	2.374	1.498		49
48	3.017	2.958	2.955	2.750	2.943	3.245	3.253	2.762	2.931	3.160	3.017	2.742	2.824	2.438	2.261	2.485	2.282	2.110	2.085	1.144	2.287	2.517	1.686		48
47	2.993	2.895	2.801	2.840	2.718	2.813	2.924	2.718	2.689	2.990	2.725	2.631	2.569	2.367	2.335	2.406	2.462	2.139	2.201	1.435	2.389	2.423	1.810	1.386	47
46	2.970	3.031	2.932	2.793	3.145	3.190	3.126	2.766	2.912	3.150	2.876	2.903	2.714	2.547	2.728	2.484	2.585	2.338	2.376	1.777	2.574	2.478	1.898	1.665	46
45	2.994	3.033	2.966	2.753	3.191	2.977	3.105	2.847	3.043	3.028	2.898	2.724	2.694	2.582	2.720	2.538	2.581	2.575	2.369	1.960	2.605	2.540	2.085	2.017	45
44	2.918	3.048	2.770	2.954	3.243	3.181	3.172	3.125	2.946	3.111	3.170	2.999	2.888	2.641	2.720	2.618	2.786	2.477	2.682	1.877	2.684	2.744	2.107	2.155	44
43	2.849	2.888	2.964	2.912	3.096	3.234	3.153	2.855	2.961	3.038	3.178	3.098	2.773	2.568	2.598	2.631	2.772	2.642	2.494	2.120	2.626	2.603	2.388	2.222	43
42	2.387			2.981	2.928	3.227	3.126	2.994	2.860	3.214	2.909	3.153	2.969	2.832	2.902	2.959	3.088	3.019	2.658	2.112	2.786	2.528	2.381	2.327	42
41	2.843			3.054	3.222	3.193	3.187	2.896	2.854	3.093	3.036	2.978	2.800	2.775	2.804	2.655	2.954	2.782	2.708	2.317	2.523	2.572	2.366	2.444	41
40	2.904			2.938	3.074	3.035	3.167	2.935	3.165	3.182	3.104	3.189	2.981	2.787	3.087	3.016	3.036	3.043	2.834	2.392	2.796	2.723	2.538	2.491	40
39								3.121	2.903	3.274	3.251	3.213	3.134	2.983	3.224	3.160	3.177	2.990	2.877	2.690	2.947	3.126	2.619	2.662	39
38												3.159	2.864	2.787	3.108	3.016	3.036	2.998	2.973	2.500	3.055	2.728	2.528	2.631	38
37												3.122	3.022	3.152	3.156	3.033	3.120	2.688	2.808	2.715	3.024	2.800	2.677	2.773	37
36													2.870	3.270	3.052	3.120	3.078	3.152	3.086	2.567	3.110	3.030	2.788	2.835	36

*degree from the east end of the equator

Table A2c. Total $1/e$-Width of Ca II H (km/sec).

traced position no.	1	2	3	4	5	6	7	8	9	10	11	12	13	14	15	16	17	18	19	20	21	22	23	24	traced position no.
position angle*	48.7	48.0	47.5	45.0	44.7	44.0	43.6	42.1	42.7	41.5	40.9	40.0	33.4	32.8	31.9	31.6	31.3	31.0	29.5	30.3	28.9	27.9	27.3	27.5	position angle*
frame no.																									frame no.
71				26.8	27.9		31.1			53.8	34.3														71
70	37.4	26.2		22.4	30.4	30.3				45.4	26.8														70
69	33.4	21.0		24.8	32.1	46.6				51.0	31.8														69
68	23.8	24.0		30.0	25.4	32.4				50.7	34.5											23.2			68
67	44.1	24.8	23.3	22.3	23.5	39.0	25.7			48.9	37.5											28.1			67
66	56.0	24.8	22.3	20.8	27.1	51.7	40.5			48.9	37.1		58.2									28.0			66
65	40.1	25.9	21.3	25.8	22.2	59.3	31.6	60.1		42.8	33.7		55.4									26.6			65
64	42.7	26.6	26.2	28.1	22.5	52.2	34.4	51.4		39.7	36.9		55.1									21.8			64
63	44.6	27.1	29.9	29.1	28.2	62.9	31.5			46.5	34.0	43.0	42.3									21.6			63
62	40.1	33.7	27.7	31.2	28.3	46.2	32.8	39.6	46.7	38.6	39.4	49.6	45.6									22.4			62
61	40.6	29.9	30.9	27.0	31.2	56.5	31.5	35.4	54.8	35.6	36.7														61
60	52.5	25.2	29.0	29.5	30.4	52.5	39.2	44.7	45.1	38.4	64.1	39.5	47.2								60.9	19.6			60
59	48.5	51.0	40.1	28.6	44.7	45.3	41.7	52.3	41.9	43.3	70.8	40.4	47.3			31.1					69.0	26.5			59
58	48.4	34.3	38.9	28.0	36.9	54.8	34.4	51.5	37.5	52.4	63.2	43.4	54.0			31.0			40.8		56.9	25.7			58
57	52.0	40.3	36.5	15.7	43.8	56.6	45.8	49.3	39.6	48.4	70.1	45.4	47.5			26.9	44.2		59.0		58.1	26.0	35.1		57
56	50.4	54.7	45.7	31.9	52.3	64.1	53.1	62.5	49.0	35.0	72.1	49.9	45.4	38.6		26.7	42.2		36.3		55.1	24.6	45.7		56
55	51.3	45.0	42.3	35.5	50.0	46.5	53.6	50.5	40.4	50.7	61.0	50.5	53.0	37.2	41.8	26.2	46.3		44.0		44.2	27.8	35.2		55
54	55.1	50.2	47.8	45.9	47.8	62.0	55.6	42.6	52.5	42.2	74.9	51.8	52.0	36.8	40.8	29.2	51.0		51.9		45.1	31.7	35.3		54
53	49.8	55.8	36.6	45.3	46.7	53.1	47.8	47.3	50.8	48.8	59.7	50.0	41.4	39.5	41.9	25.9	53.9		45.4		48.6	29.2	35.4		53
52	57.4	50.6	41.6	39.7	46.1	58.6	52.1	54.1	51.3	56.6	70.6	46.2	50.2	41.1	37.6	32.6	46.6	28.6	40.4		44.6	31.2	35.8		52
51	53.4	49.0	47.6	50.1		51.3	44.7	43.0	40.0	51.0	70.6	59.0	55.1	44.8	41.0	34.7	53.2	30.6	35.5		39.8	24.8	38.0		51
50	63.2	64.0	36.4	41.0	50.8	70.5	56.8	56.9	53.6	56.5	71.5	48.1	53.0	38.0	35.4	29.3	47.0	40.2	53.3		39.9	24.1	36.8		50
49	43.6	57.2	46.3	61.8	65.5	66.5	49.0	48.8	55.6	53.1	65.6	64.3	38.6	33.2	42.7	27.8	56.1	40.5	38.2	35.6	49.2	30.4	33.1		49
48	55.0	56.7	46.3	55.3	52.0	62.2	52.5	59.1	51.4	57.0	63.8	54.0	30.4	35.4	42.0	38.5	63.3	34.8	41.6	38.9	45.4	28.8	39.0		48
47	59.8	62.8	54.3	46.8	67.7	64.4	61.9	62.5	62.9	57.7	69.9	66.5	44.6	33.5	49.8	46.7	56.3	45.8	43.0	42.6	39.1	33.0	32.6	33.6	47
46	62.4	66.2	56.6	56.5	31.7	55.3	63.4	62.4	33.2	58.8	66.1	47.7	49.3	38.6	36.0	53.6	63.0	42.4	46.0	39.2	27.9	35.2	38.2	31.2	46
45	64.3	67.7	56.0	56.8	47.0	61.4	69.6	67.2	57.9	63.2	68.3	70.5	54.6	43.8	43.7	48.1	65.3	36.0	49.2	39.4	31.5	40.2	42.2	36.7	45
44	71.6	53.5	62.1	56.7	40.6	64.8	57.2	58.6	62.6	64.2	62.7	68.5	49.3	42.5	54.6	55.1	54.0	51.0	36.6	46.7	40.5	29.5	46.5	41.0	44
43	69.1	69.2	52.6	51.1	53.0	49.5	60.1	56.7	61.5	66.9	68.3	56.1	49.9	49.0	63.9	55.5	61.0	50.3	52.9	46.2	41.5	37.9	34.7	48.4	43
42	64.1			61.7	60.1	60.7	66.3	62.4	66.6	65.5	80.0	64.5	48.2	51.3	55.6	53.5	49.4	38.7	43.6	48.9	42.8	51.6	45.6	51.3	42
41	68.0			62.3	72.7	77.1	69.6	69.4	66.1	72.9	73.0	66.6	55.6	60.6	57.3	68.0	56.3	45.9		52.5	54.8	38.0	48.8	46.2	41
40	62.7			72.5	49.2	65.1	78.3	76.2	52.9	65.3	73.1	66.1	54.5	66.7	60.0	56.5	54.5	44.6	56.9	51.1	54.2	41.9	44.2	48.4	40
39								52.0	71.4	75.9	62.7	62.8	62.1	65.2	65.1	55.4	55.6	51.4	59.0	40.6	45.1	33.4	50.0	49.6	39
38												69.9	61.3	65.4	61.7	71.0	69.7	60.6	49.4	60.0	44.6	56.2	57.3	57.0	38
37												69.7	61.6	58.5	63.0	66.6	72.1	75.1	70.0	48.4	49.2	53.0	59.0	52.0	37
36													75.5	53.8	76.5	73.5	75.8	77.8	49.6	61.2	46.5	49.8	48.5	44.8	36

*degree from the east end of the equator

Table A3a. Total Intensity ($\log E - 10$) of CaII K (erg/sec.cm.ster).

traced position no.	1	2	3	4	5	6	7	8	9	10	11	12	13	14	15	16	17	18	19	20	21	22	23	24	traced position no.
position angle*	48.7	48.0	47.5	45.0	44.7	44.0	43.6	42.1	42.7	41.5	40.9	40.0	33.4	32.8	31.9	31.6	31.3	31.0	29.5	30.3	28.9	27.9	27.3	27.5	position angle*
frame no.																									frame no.
71				1.128	1.679	0.985	1.287			2.314	1.543														71
70	0.959	1.247		1.355	1.735		1.527			2.301	1.684														70
69	1.596	1.569		1.455	1.820	1.560	1.509			2.294	1.746														69
68	1.554	1.805		1.456	1.917	1.773	1.642			2.488	2.018											1.381			68
67	1.903	2.099	1.439	1.820	2.182	1.868	1.732			2.472	2.103		1.411									1.576			67
66	2.087	2.242	1.639	1.863	2.162	1.894	1.761			2.541	2.255		1.635									1.780			66
65	2.209	2.333	1.912	1.994	2.138	1.973	1.810	1.713		2.562	2.294		1.644									1.905			65
64	2.417	2.531	2.032	2.143	2.358	2.358	1.935	1.871		2.559	2.402		1.748									2.119			64
63	2.735	2.685	2.337	2.527	2.540	2.567	2.226	2.082		2.690	2.407	1.681	2.066									2.405			63
62	2.819	2.754	2.314	2.442	2.587	2.677	2.487	2.152	2.094	2.732	2.495	1.954	2.156									2.249			62
61	2.953	2.803	2.636	2.612	2.739	2.856	2.570	2.257	2.341	2.751	2.537	2.168	2.336									2.554			61
60	3.084	2.938	2.634	2.582	2.773	3.069	2.651	2.346	2.530	2.727	2.654	2.285	2.479								2.061	2.598			60
59	3.078	2.951	2.895	2.665	2.898	3.101	2.925	2.599	2.709	2.792	2.765	2.442	2.540			1.425					2.291	2.691			59
58	3.436	3.348	2.919	3.060	3.091	3.223	3.209	2.864	2.940	3.081	3.056	2.731	2.738			1.659			1.309		2.505	2.763			58
57	3.420	3.292	3.113	2.905	3.208	3.329	3.177	2.946	3.048	3.143	3.097	2.813	2.806			1.866	1.757		1.807		2.630	2.833	1.381		57
56	3.381	3.302	3.189	3.134	3.251	3.521	3.392	3.242	3.192	3.335	3.220	2.977	2.928	1.761		2.100	1.996		2.033		2.685	2.903	1.502		56
55	3.502	3.452	3.338	3.225	3.311	3.603	3.412	3.244	3.159	3.391	3.424	3.146	2.995	2.004	1.806	2.178	2.230		2.200		2.836	3.033	1.627		55
54	3.586	3.576	3.339	3.332	3.459	3.737	3.630	3.444	3.255	3.463	3.508	3.214	3.118	2.265	2.152	2.324	2.383		2.267		2.750	2.920	1.701		54
53	3.580	3.605	3.460	3.418	3.505	3.655	3.666	3.396	3.318	3.494	3.505	3.287	3.099	2.444	2.397	2.402	2.583		2.436		2.857	3.026	1.808		53
52	3.778	3.603	3.446	3.469	3.454	3.701	3.760	3.557	3.492	3.613	3.563	3.433	3.204	2.590	2.571	2.614	2.747	2.157	2.491		2.924	3.029	1.739		52
51	3.726	3.763	3.510	3.577	3.783	3.757	3.847	3.682	3.599	3.760	3.833	3.594	3.513	2.853	2.766	2.897	2.963	2.466	2.734		3.049	3.236	2.070		51
50	3.840	3.848	3.556	3.592	3.778	3.897	3.822	3.732	3.633	3.854	3.739	3.610	3.629	2.962	2.879	3.015	3.147	2.649	2.826		3.200	3.407	2.240		50
49	3.845	3.883	3.671	3.691	3.886	3.900	3.817	3.846	3.812	3.876	3.826	3.672	3.700	3.149	3.033	3.331	3.215	2.815	2.886	1.852	3.233	3.178	2.473		49
48	3.959	3.853	3.852	3.864	3.901	4.143	4.155	4.009	3.833	4.124	3.974	3.856	3.591	3.292	3.352	3.357	3.578	2.916	3.129	2.161	3.248	3.508	2.564		48
47	3.953	3.806	3.756	3.667	3.814	4.018	3.890	3.903	3.813	3.963	3.753	3.743	3.612	3.460	3.284	3.555	3.453	3.057	3.168	2.402	3.418	3.388	2.812	2.429	47
46	4.045	3.843	3.840	3.902	3.996	4.226	4.087	3.913	3.963	4.107	4.078	4.082	3.690	3.531	3.496	3.768	3.703	3.366	3.374	2.718	3.393	3.477	2.970	2.640	46
45	4.088	3.922	3.820	3.828	3.938	4.110	4.141	3.882	4.097	4.145	3.996	3.960	3.883	3.607	3.470	3.603	3.886	3.446	3.265	2.866	3.477	3.486	3.012	2.865	45
44	4.184	4.035	4.004	3.942	4.015	4.166	4.219	3.975	4.150	4.122	3.988	3.805	3.846	3.529	3.606	3.738	3.727	3.462	3.554	2.985	3.527	3.473	3.112	3.114	44
43	4.012	3.929	3.955	3.970	3.911	4.039	4.097	4.078	4.086	4.125	4.162	3.994	3.851	3.660	3.843	3.655	3.925	3.757	3.512	3.082	3.593	3.671	3.267	3.088	43
42	4.083			3.970	3.973	4.140	4.095	3.980	4.071	4.091	3.905	3.936	3.823	3.803	3.910	3.924	4.000	3.832	3.677	3.194	3.785	3.702	3.365	3.259	42
41	3.875			3.997	4.058	4.206	4.153	4.213	4.190	4.173	4.186	4.003	3.970	3.943	3.933	3.931	4.164	3.748	3.796	3.304	3.758	3.726	3.348	3.422	41
40	3.796			4.131	3.988	3.959	4.305	4.138	4.071	4.304	4.189	4.079	3.960	3.815	3.993	3.877	4.105	3.758	3.885	3.338	3.760	3.748	3.618	3.564	40
39								4.232	4.082	4.141	4.242	4.203	4.175	3.982	4.033	4.098	4.108	3.897	3.939	3.400	3.813	3.748	3.601	3.777	39
38												4.131	4.062	4.030	4.185	4.006	4.095	3.927	3.986	3.640	3.996	3.864	3.659	3.676	38
37												4.079	3.996	4.026	4.085	4.055	4.213	4.061	3.889	3.624	4.064	3.976	3.693	3.810	37
36													4.149	4.100	4.222	4.122	4.246	3.939	4.051	3.784	4.011	3.984	3.675	3.799	36

*degree from the east end of the equator

Table A3b. Peak Intensity ($log E_0 - 19$) of Ca II K (erg/sec.cm.ster.cm).

traced position no.	1	2	3	4	5	6	7	8	9	10	11	12	13	14	15	16	17	18	19	20	21	22	23	24	traced position no.
position angle*	48.7	48.0	47.5	45.0	44.7	44.0	43.6	42.1	42.7	41.5	40.9	40.0	33.4	32.8	31.9	31.6	31.3	31.0	29.5	30.3	28.9	27.9	27.3	27.5	position angle*
frame no.																									frame no.
71				0.719	1.231	0.331	0.672			1.602	0.882														71
70	0.555	0.899		0.905	1.174		0.896			1.584	1.051														70
69	0.959	1.201		1.010	1.410	0.839	0.947			1.534	1.111														69
68	1.000	1.393		1.164	1.511	0.991	0.999			1.715	1.393		0.556									0.795			68
67	1.125	1.584	1.106	1.514	1.660	1.083	1.065			1.717	1.454		0.598									1.178			67
66	1.354	1.712	1.216	1.512	1.674	1.214	1.158			1.823	1.625		0.882									1.306			66
65	1.441	1.826	1.523	1.727	1.680	1.176	1.165	0.804		1.818	1.620		0.897									1.381			65
64	1.571	1.971	1.570	1.769	1.854	1.501	1.283	1.137		1.872	1.689		1.012									1.744			64
63	1.935	1.994	1.744	1.866	2.005	1.718	1.636	1.323		1.939	1.688	0.885	1.388									2.009			63
62	2.042	2.089	1.801	1.988	1.980	1.929	1.901	1.526	1.412	2.083	1.756	1.266	1.400									1.911			62
61	2.255	2.170	2.030	2.111	2.081	2.001	1.895	1.644	1.623	1.960	1.769	1.436	1.634									2.199			61
60	2.273	2.328	1.986	2.070	2.048	2.287	1.944	1.616	1.816	2.036	1.796	1.621	1.772								1.192	2.172			60
59	2.348	2.207	2.265	1.973	2.162	2.292	2.207	1.813	1.924	1.990	1.788	1.703	1.707			0.880					1.445	2.168			59
58	2.607	2.582	2.235	2.581	2.326	2.317	2.473	2.023	2.180	2.318	2.086	1.989	1.944			1.157			0.802		1.657	2.268			58
57	2.537	2.555	2.436	2.162	2.518	2.398	2.463	1.967	2.301	2.313	2.151	1.988	2.015			1.362	1.035		1.041		1.812	2.350	0.726		57
56	2.516	2.530	2.447	2.385	2.554	2.659	2.515	2.322	2.400	2.468	2.247	2.188	2.158	1.119		1.602	1.174		1.266		1.948	2.409	0.804		56
55	2.663	2.646	2.566	2.516	2.566	2.956	2.573	2.353	2.441	2.490	2.515	2.332	2.345	1.392	1.198	1.673	1.458		1.470		2.119	2.490	0.995		55
54	2.649	2.789	2.593	2.548	2.742	2.916	2.660	2.584	2.648	2.577	2.605	2.415	2.331	1.586	1.454	1.778	1.638		1.560		2.134	2.312	1.075		54
53	2.806	2.784	2.688	2.695	2.654	2.770	2.955	2.563	2.492	2.615	2.523	2.399	2.445	1.802	1.694	1.819	1.830		1.720		2.072	2.424	1.207		53
52	2.899	2.805	2.685	2.713	2.632	2.856	2.948	2.629	2.706	2.658	2.545	2.479	2.417	1.919	1.899	2.025	1.977	1.556	1.749		2.142	2.409	1.127		52
51	2.805	2.902	2.784	2.804	2.952	2.862	2.899	2.788	2.720	2.938	2.856	2.670	2.800	2.135	2.051	2.363	2.105	1.797	2.011		2.329	2.715	1.468		51
50	3.026	3.046	2.780	2.749	3.044	2.988	3.038	2.840	2.843	3.013	2.724	2.832	2.794	2.291	2.154	2.319	2.284	2.001	2.080		2.523	2.898	1.628		50
49	2.902	3.016	2.869	2.827	3.019	2.959	2.896	3.037	2.929	2.883	2.826	2.848	2.881	2.389	2.326	2.571	2.241	2.069	2.068	1.098	2.500	2.563	1.752		49
48	3.083	3.044	3.059	3.046	3.037	3.286	3.287	3.085	2.930	3.322	2.971	3.023	2.781	2.586	2.590	2.716	2.600	2.170	2.380	1.352	2.540	2.934	1.911		48
47	3.085	2.963	2.970	2.811	2.974	3.141	3.019	3.043	2.911	2.965	2.673	2.813	2.925	2.723	2.515	2.831	2.517	2.359	2.483	1.661	2.833	2.695	1.983	1.741	47
46	3.183	3.020	2.998	3.096	3.149	3.300	3.261	2.963	3.143	3.221	3.158	3.192	2.799	2.787	2.642	3.090	2.869	2.685	2.544	2.001	2.594	2.839	2.276	1.958	46
45	3.125	3.008	2.913	3.035	3.074	3.169	3.233	3.031	3.177	3.281	3.056	2.927	2.934	2.793	2.538	2.772	2.875	2.658	2.470	2.110	2.736	2.845	2.242	2.135	45
44	3.274	2.991	3.183	3.120	3.106	3.250	3.285	3.031	3.208	3.211	2.953	2.804	3.000	2.630	2.724	3.025	2.757	2.595	2.668	2.285	2.837	2.733	2.329	2.376	44
43	3.182	3.110	3.250	3.110	2.979	3.214	3.143	3.207	3.183	3.207	3.214	3.032	3.065	2.778	2.942	2.695	2.972	2.894	2.628	2.319	2.931	3.031	2.480	2.326	43
42	3.076			2.997	3.124	3.243	3.182	3.067	3.196	3.044	2.883	2.977	2.881	2.812	2.937	3.013	3.003	2.931	2.881	2.412	3.107	3.086	2.532	2.435	42
41	3.080			3.005	3.051	3.241	3.165	3.307	3.173	3.205	3.191	3.006	3.140	2.960	2.931	3.011	3.306	2.822	2.966	2.493	3.022	2.928	2.495	2.654	41
40	2.755			3.148	3.155	3.020	3.296	3.152	3.050	3.266	3.205	3.037	3.070	2.899	3.076	2.950	3.085	2.766	2.992	2.570	2.895	3.071	2.890	2.672	40
39								3.198	3.154	3.105	3.217	3.283	3.244	2.936	3.095	3.205	3.252	2.959	3.038	2.486	2.994	2.867	2.753	2.948	39
38												3.149	3.044	3.032	3.217	3.065	2.945	2.937	3.141	2.797	3.110	2.892	2.792	2.720	38
37												3.018	2.964	3.012	3.016	3.084	3.236	3.254	2.915	2.685	3.308	3.198	2.768	2.821	37
36													3.193	3.170	3.283	3.132	3.201	2.886	3.224	2.775	3.107	2.867	2.856	2.910	36

*degree from the east end of the equator

Table A3c. Total 1/e-Width of Ca II K (km/sec).

traced position no.	1	2	3	4	5	6	7	8	9	10	11	12	13	14	15	16	17	18	19	20	21	22	23	24	traced position no.
position angle*	48.7	48.0	47.5	45.0	44.7	44.0	43.6	42.1	42.7	41.5	40.9	40.0	33.4	32.8	31.9	31.6	31.3	31.0	29.5	30.3	28.9	27.9	27.3	27.5	position angle*
frame no.																									frame no.
71				20.3	22.3		21.2			46.6	38.6														71
70	20.0			21.4	29.4		26.4			48.2	33.6														70
69		19.7		21.7	22.2	41.7	30.2			51.7	32.2														69
68		21.6		17.5	26.0	55.0	38.6			55.3	36.7											32.0			68
67	52.8	24.7	17.2	17.8	23.4	56.0	37.7			49.5	33.0		57.0									21.2			67
66	46.2	26.9	21.1	19.0	21.2	42.6	31.6			44.2	36.3		50.0									25.6			66
65	52.5	26.4	18.3	14.7	20.4	51.1	35.1	51.7		42.4	34.5		49.3									26.2			65
64	63.1	28.4	22.5	17.8	23.2	58.7	32.9	46.7		36.2	38.7		48.0									20.4			64
63	52.2	43.6	33.4	37.5	23.2	59.8	29.7	46.5		46.2	40.8	51.7	43.8									19.5			63
62	47.8	32.2	26.6	22.0	28.1	43.0	31.6	30.4	39.9	32.1	42.1	42.7	49.0									16.1			62
61	39.8	34.8	33.4	25.3	34.3	58.4	30.2	31.4	38.7	47.5	45.2	45.5	41.0									19.8			61
60	45.8	30.6	34.5	25.6	42.4	51.0	41.2	41.4	43.5	39.2	60.5	38.3	42.8								47.8	21.0			60
59	38.4	44.5	33.1	34.8	44.3	52.0	46.5	52.6	49.1	50.8	77.2	43.9	57.6			29.3					61.5	29.3			59
58	46.4	35.3	38.9	20.0	49.7	63.8	37.7	51.7	44.4	45.3	80.0	43.7	54.5			27.0			34.4		57.8	25.3			58
57	53.4	38.1	36.7	46.5	40.2	70.0	42.3	67.6	43.9	52.2	73.9	54.2	52.6			26.0	47.3		48.1		55.6	22.6	37.2		57
56	60.0	51.4	42.3	39.7	41.6	63.4	48.7	57.8	42.9	45.2	75.0	51.2	49.8	36.9		25.0	58.3		48.7		45.9	22.0	42.2		56
55	58.3	51.2	43.7	36.6	44.6	35.3	54.7	55.0	41.4	62.2	72.1	52.1	39.1	34.4	34.7	25.9	51.8		46.2		43.0	28.9	36.8		55
54	70.4	46.3	44.8	48.9	48.2	54.5	52.0	52.5	41.0	52.4	59.5	52.1	55.0	42.7	42.3	28.8	44.1		41.9		45.7	30.8	34.4		54
53	62.1	57.1	46.7	41.6	59.5	66.0	38.1	58.5	48.6	59.7	75.1	60.1	36.8	37.8	44.8	32.0	43.7		42.6		48.5	29.2	35.4		53
52	63.5	55.0	47.9	45.9	67.0	61.1	50.9	53.6	50.7	62.8	73.8	62.6	48.9	40.2	42.2	34.7	49.0	28.4	47.1		53.5	33.8	33.3		52
51	68.0	57.5	50.1	49.2	57.4	66.2	65.0	51.9	54.9	50.8	60.1	59.6	37.6	40.5	40.8	27.2	57.7	36.9	43.6		43.9	23.4	31.7		51
50	60.0	56.3	56.1	56.0	41.4	68.8	58.9	55.5	50.7	50.2	68.0	43.3	44.0	34.8	43.1	44.2	60.1	41.1	52.3		36.7	22.1	29.9		50
49	69.8	63.0	60.5	61.7	64.7	77.7	67.2	54.3	62.3	70.0	72.1	52.1	42.2	49.7	40.6	46.6	77.6	48.6	54.5	48.9	45.4	44.0	37.5		49
48	68.6	58.1	52.1	47.7	61.8	63.9	74.6	65.3	59.0	48.6	71.8	54.5	49.6	37.8	41.8	35.9	51.9	43.6	44.8	50.3	42.0	26.4	36.6		48
47	62.7	68.1	47.2	58.1	58.3	69.4	67.7	58.3	61.3	74.3	82.6	60.5	48.9	33.7	45.5	30.0	72.4	39.4	41.1	45.0	28.9	29.9	53.1	39.5	47
46	61.3	55.6	61.2	56.0	61.7	75.8	56.3	65.5	53.7	54.7	73.5	65.2	60.1	44.2	52.3	37.7	56.2	40.8	51.2	43.0	50.4	31.6	39.0	38.7	46
45	68.8	64.2	65.2	52.1	63.1	75.3	70.4	58.1	69.9	56.1	71.7	63.1	74.3	43.8	65.1	51.1	72.0	46.8	50.3	46.8	40.3	29.1	45.2	42.3	45
44	67.6		57.0	57.4	70.4	67.9	74.5	74.5	68.7	66.3	76.5	74.1	51.8	62.7	56.5	39.0	75.0	50.5	57.1	42.3	40.2	43.8	47.7	38.8	44
43	64.9			63.8	79.1	78.4	66.1	64.6	67.0	75.0	72.3	76.4	51.1	58.5	62.3	64.3	71.6	49.4	60.1	50.3	34.1	28.8	44.0	46.3	43
42	81.5			69.3	64.0	65.0	73.5	58.9	57.7	70.2	76.2	72.7	68.7	64.6	73.0	58.0	76.5	53.5	41.4	47.6	36.0	27.8	51.7	51.5	42
41	64.6			65.0	73.1	75.3	66.9	66.4	74.8	62.5	72.1	86.7	60.8	67.5	74.0	60.6	57.2	67.1	53.1	51.7	38.8	42.0	57.0	42.8	41
40				67.0	51.1	76.0	81.0	62.8	71.1	68.7	74.0	83.3	57.0	58.2	65.8	71.2	78.4	67.0	57.1	49.6	53.7	36.8	31.2	57.2	40
39								80.7	65.0	80.8	79.1	74.9	63.6	79.5	75.0	68.7	62.1	59.4	61.9	58.8	44.4	56.1	60.2	47.7	39
38												66.6	72.3	73.9	74.1	69.5	91.3	65.6	54.4	47.9	55.6	54.5	54.1	62.3	38
37												83.8	72.9	73.0	80.4	67.0	81.9	55.0	75.0	65.1	48.9	47.2	61.9	65.3	37
36													71.0	60.8	64.6	76.9	86.3	78.1	55.5	66.3	60.1	60.9	52.5	66.1	36

*degree from the east end of the equator

Table A4a. Total Intensity ($\log E - 10$) of Hε (erg/sec.cm.ster).

traced position no.	1	2	3	4	5	6	7	8	9	10	11	12	13	14	15	16	17	18	19	20	21	22	23	24	traced position no.
position angle*	48.7	48.0	47.5	45.0	44.7	44.0	43.6	42.1	42.7	41.5	40.9	40.0	33.4	32.8	31.9	31.6	31.3	31.0	29.5	30.3	28.9	27.9	27.3	27.5	position angle*
frame no.																									frame no.
63	0.879																								63
62	1.079					0.905				1.019															62
61	1.109					0.731				1.078															61
60	1.417	1.062	0.518			1.193	1.063																		60
59	1.682	1.512	0.974	1.039	1.108	1.499	1.425			1.245	0.863	0.763										1.049			59
58	1.850	1.539	1.174	1.135	1.397	1.644	1.561	1.279	1.366	1.496	1.376	0.866													58
57	1.984	1.773	1.596	1.267	1.624	1.790	1.743	1.603	1.470	1.615	1.604	1.071	1.011									0.990			57
56	2.208	2.062	1.746	1.402	1.731	1.925	1.895	1.621	1.463	1.756	1.679	1.322										0.828			56
55	2.382	2.190	1.966	1.658	1.883	2.001	2.032	1.939	1.580	1.954	1.956	1.517										1.106			55
54	2.508	2.350	2.027	1.804	2.078	2.252	2.168	1.941	1.860	2.112	2.037	1.663	1.137												54
53	2.694	2.512	2.316	1.962	2.314	2.401	2.366	2.142	1.994	2.250	2.217	1.760	1.439												53
52	2.823	2.690	2.530	2.082	2.323	2.445	2.469	2.175	2.172	2.383	2.350	1.950	1.495									1.027			52
51	2.968	2.890	2.660	2.217	2.588	2.655	2.667	2.368	2.289	2.531	2.443	2.112	1.627									1.316			51
50	3.131	3.008	2.859	2.386	2.694	2.818	2.809	2.520	2.426	2.714	2.658	2.286	1.793	1.347	1.537	1.268	1.528					1.431			50
49	3.296	3.057	2.954	2.620	2.784	2.955	2.992	2.646	2.524	2.846	2.757	2.390	1.880	1.543	1.684	1.565	1.644					1.265			49
48	3.478	3.446	3.141	2.763	3.054	3.096	3.181	2.848	2.853	2.983	3.016	2.516	1.973	1.706	1.815	1.858	1.890	1.343			1.599	1.738			48
47	3.482	3.368	3.289	2.893	3.074	3.164	3.134	2.972	3.019	3.227	3.083	2.709	2.118	1.890	2.097	1.970	2.133	1.651			1.592	1.630			47
46	3.506	3.551	3.444	3.018	3.234	3.350	3.400	3.033	3.166	3.243	3.293	2.975	2.261	2.167	2.298	2.308	2.408	1.972	1.632		1.553	1.480			46
45	3.721	3.535	3.571	3.219	3.405	3.439	3.374	3.192	3.199	3.411	3.354	3.055	2.363	2.341	2.550	2.405	2.650	2.199	1.684	1.446	1.767	1.676	1.118	1.299	45
44	3.851	3.703	3.644	3.256	3.497	3.783	3.558	3.503	3.251	3.487	3.662	3.294	2.560	2.522	2.647	2.582	2.763	2.405	1.921	1.421	1.937	1.733	1.559	1.672	44
43	3.632	3.556	3.535	3.400	3.471	3.681	3.718	3.511	3.626	3.494	3.508	3.398	2.721	2.652	2.813	2.748	2.938	2.590	2.028	1.618	2.158	1.945	1.802	2.041	43
42	3.818			3.504	3.616	3.667	3.695	3.540	3.637	3.558	3.674	3.554	2.847	2.934	3.054	2.917	3.136	2.805	2.234	1.715	2.168	1.936	1.863	1.956	42
41				3.605	3.670	3.754	3.809	3.558	3.688	3.712	3.546	3.578	2.998	3.030	3.183	3.094	3.235	3.071	2.482	2.046	2.330	2.051	1.880	2.131	41
40				3.770	3.570	3.600	3.854	3.776	3.633	3.748	3.740	3.721	3.136	3.094	3.338	3.264	3.472	3.192	2.671	2.268	2.521	2.137	2.100	2.293	40
39								3.768	3.980	4.081	3.964	3.780	3.358	3.378	3.648	3.499	3.666	3.389	2.931	2.576	2.748	2.442	2.343	2.533	39
38												3.864	3.313	3.445	3.678	3.572	3.557	3.293	3.025	2.649	2.631	2.662	2.253	2.641	38
37												3.777	3.505	3.607	3.762	3.739	3.800	3.491	3.204	2.935	3.012	2.747	2.608	2.867	37
36													3.498	3.653	3.843	3.774	3.774	3.807	3.271	3.150	3.292	2.783	2.652	2.935	36

*degree from the east end of the equator

Table A4b. Peak Intensity ($log E_0 - 19$) of Hε (erg/sec.cm.ster.cm).

traced position no.	1	2	3	4	5	6	7	8	9	10	11	12	13	14	15	16	17	18	19	20	21	22	23	24	traced position no.
position angle*	48.7	48.0	47.5	45.0	44.7	44.0	43.6	42.1	42.7	41.5	40.9	40.0	33.4	32.8	31.9	31.6	31.3	31.0	29.5	30.3	28.9	27.9	27.3	27.5	position angle*
frame no.																									frame no.
63	0.185																								63
62	0.288					0.131				0.322															62
61	0.487					0.052				0.276															61
60	0.649	0.385	0.048			0.414	0.537																		60
59	0.862	0.675	0.326	0.310	0.434	0.677	0.651		0.338	0.513	−0.14	0.083	0.138									0.357			59
58	1.032	0.782	0.592	0.486	0.584	0.842	0.827	0.477	0.610	0.803	0.526	0.210	0.233									0.530			58
57	1.239	1.048	0.893	0.596	0.922	0.945	1.092	0.807	0.682	0.946	0.814	0.247	0.400									0.425			57
56	1.497	1.297	1.130	0.808	1.034	1.150	1.172	0.928	0.807	1.060	0.874	0.579										0.334			56
55	1.701	1.547	1.372	0.990	1.152	1.287	1.357	1.140	0.941	1.134	1.119	0.736	0.335									0.331			55
54	1.812	1.677	1.486	1.142	1.379	1.507	1.411	1.216	1.218	1.454	1.242	0.925	0.529												54
53	2.025	1.808	1.706	1.291	1.637	1.616	1.669	1.356	1.314	1.551	1.405	0.977	0.710												53
52	2.104	1.979	1.906	1.351	1.624	1.716	1.780	1.430	1.500	1.683	1.591	1.218	0.739									0.517			52
51	2.262	2.130	1.978	1.562	1.913	1.892	1.923	1.617	1.546	1.901	1.749	1.391	0.921				0.349					0.698			51
50	2.449	2.315	2.231	1.772	1.981	2.105	2.081	1.825	1.746	1.965	1.900	1.548	1.139	0.641	0.796	0.766	0.681					0.823			50
49	2.628	2.336	2.375	1.974	2.075	2.190	2.351	1.893	1.802	2.178	1.939	1.661	1.187	0.818	1.037	0.922	0.795					0.626			49
48	2.723	2.763	2.466	2.144	2.368	2.388	2.563	2.097	2.137	2.371	2.421	1.733	1.297	0.998	1.178	1.105	1.119	0.616			0.824	0.805			48
47	2.757	2.671	2.565	2.319	2.419	2.474	2.300	2.207	2.316	2.541	2.313	2.005	1.399	1.191	1.453	1.413	1.398	1.036	0.652		0.818	0.878			47
46	2.816	2.912	2.801	2.322	2.640	2.735	2.699	2.330	2.496	2.495	2.545	2.264	1.513	1.473	1.666	1.605	1.582	1.335	0.820	0.469	0.794	0.935			46
45	2.971	2.764	2.790	2.510	2.805	2.761	2.569	2.413	2.375	2.673	2.627	2.323	1.660	1.677	1.816	1.676	1.885	1.491	0.909	0.743	1.017	1.043	0.606	0.712	45
44	3.198	2.936	2.933	2.679	2.723	3.101	2.871	2.745	2.432	2.800	2.989	2.557	1.834	1.784	1.865	1.922	1.969	1.660	1.174	0.762	1.232	1.103	0.787	0.928	44
43	2.931	2.720	2.873	2.693	2.809	3.093	2.999	2.657	2.934	2.722	2.781	2.673	2.050	1.957	1.985	2.047	2.123	1.902	1.291	0.964	1.383	1.115	1.045	1.243	43
42	3.207			2.830	2.972	3.120	3.010	2.733	2.927	2.851	2.944	2.722	2.095	2.216	2.297	2.129	2.445	2.036	1.488	0.977	1.469	1.191	1.091	1.318	42
41	2.812			3.045	2.927	2.934	3.080	2.696	3.009	2.986	2.745	2.727	2.377	2.287	2.451	2.273	2.425	2.395	1.734	1.329	1.604	1.315	1.165	1.475	41
40	2.918			2.987	2.872	2.734	3.015	2.921	2.856	2.967	3.037	2.919	2.419	2.361	2.586	2.421	2.694	2.458	1.944	1.511	1.796	1.460	1.352	1.673	40
39								2.723	3.271	3.320	3.175	2.909	2.657	2.613	2.818	2.727	2.830	2.757	2.183	1.860	1.970	1.638	1.610	1.814	39
38												2.995	2.513	2.590	2.881	2.737	2.793	2.554	2.344	1.874	1.888	1.946	1.583	1.989	38
37												3.053	2.761	2.822	3.009	2.847	2.917	2.633	2.427	2.192	2.288	1.995	1.867	2.092	37
36													2.740	2.854	3.159	2.988	2.975	3.231	2.567	2.461	2.576	1.988	1.972	2.165	36

*degree from the east end of the equator

Table A4c. Total $1/e$-Width of $H\varepsilon$ (km/sec).

traced position no.	1	2	3	4	5	6	7	8	9	10	11	12	13	14	15	16	17	18	19	20	21	22	23	24	traced position no.
position angle*	48.7	48.0	47.5	45.0	44.7	44.0	43.6	42.1	42.7	41.5	40.9	40.0	33.4	32.8	31.9	31.6	31.3	31.0	29.5	30.3	28.9	27.9	27.3	27.5	position angle*
frame no.																									frame no.
63																									63
62						38.8				44.1															62
61	39.4									59.8															61
60	41.5	38.4				49.7	27.6																		60
59	50.1	51.8	37.0	42.5	45.0	63.0	45.0			43.9												43.3			59
58	51.7	49.2	33.4	34.3	54.2	48.2	45.4	52.4	43.5	42.0	62.5														58
57	44.0	41.4	40.1	40.7	40.2	56.4	38.1	51.7	47.7	42.2	60.2		35.2									28.0			57
56	44.7	48.6	35.9	35.0	38.4	49.8	42.1	43.7	37.5	43.0	67.0	51.1													56
55	39.3	38.3	36.7	40.7	48.2	47.4	40.9	52.4	33.4	58.0	59.7	48.9													55
54	39.1	41.6	34.6	43.0	36.2	43.6	47.2	45.9	40.5	36.8	54.5	46.0													54
53	35.2	40.5	32.8	38.8	36.0	50.3	40.2	53.4	41.8	39.1	52.1	52.6	43.5												53
52	42.6	42.0	33.5	44.8	40.1	41.0	41.0	43.2	37.1	47.4	50.3	43.3	46.1												52
51	38.9	48.1	35.6	36.7	37.9	46.7	45.2	45.6	45.1	31.8	42.4	39.8	45.0									36.4			51
50	38.8	43.0	37.0	33.1	38.8	42.6	43.2	42.8	39.4	42.1	42.0	44.8	41.8	40.4	45.2	26.2	54.4					32.6			50
49	35.4	45.8	37.0	34.1	41.6	45.2	32.8	46.9	42.0		50.0	39.1	43.7	41.8	40.5	36.9	57.0					36.3			49
48	42.5	36.7	36.3	34.8	37.8	39.8	38.2	41.0	39.0	32.4	31.4	56.9	42.4	44.8	36.6	47.6	44.6				48.2	64.0			48
47	43.2	41.6	41.3	29.7	37.2	40.4	51.9	43.6	35.1	37.2	43.9	43.2	52.4	41.6	33.4	32.2	41.5	33.7			53.4	47.8			47
46	38.4	36.6	35.8	40.0	26.5	33.0	34.4	35.8	34.3	43.2	40.8	46.7	41.9	41.2	34.9	39.5	53.5	39.7	53.7		46.5	29.5			46
45	40.5	46.6	41.7	40.7	33.0	37.9	47.4	45.8	51.7	43.4	43.3	46.2	40.0	36.3	45.2	41.8	46.5	40.8	51.9	42.2	51.4	38.3	29.2	30.3	45
44	30.3	43.6	34.5	30.2	45.7	41.3	38.9	40.8	48.7	37.4	33.8	42.8	42.4	38.0	47.2	41.6	52.4	43.1	46.3	40.6	41.7	36.0	51.6	46.5	44
43	42.0	41.8	43.0	43.4	33.9	31.2	36.4	42.7	36.2	48.1	36.1	37.2	38.3	41.8	49.8	44.2	48.4	42.5	44.6	31.8	50.2	60.4	28.8	49.0	43
42	28.9			39.6	34.8	31.8	38.4	43.8	36.4	40.0	40.8	47.7	39.7	44.0	42.4	50.5	38.0	50.3	43.3	44.6	43.3	46.0	46.6	35.9	42
41	35.4			26.8	40.0	43.5	41.8	50.0	37.2	44.1	45.6	44.6	35.2	45.2	44.1	51.0	39.9	36.2	46.5	42.6	44.8	46.0	41.2	37.6	41
40	57.5			46.0	37.6	52.6	50.3	40.9	39.6	41.4	31.4	47.4	32.4	46.1	49.3	50.6	39.8	39.6	42.2	46.7	42.5	37.2	45.6	33.5	40
39								62.2	35.7	46.9	41.9	51.0	35.1	44.5	45.7	43.2	47.5	35.1	43.0	41.8	47.8	47.6	49.0	42.8	39
38												53.0	46.3	53.2	46.2	48.9	42.5	45.8	37.6	45.6	47.8	42.5	45.9	36.8	38
37												39.8	41.2	43.7	36.8	46.8	52.5	44.8	42.5	42.9	40.3	40.1	44.6	48.5	37
36													41.8	51.9	31.8	38.2	52.7	29.0	39.3	38.0	40.4	50.2	41.1	45.0	36

*degree from the east end of the equator

Table A5. Mean Emission Gradients of Balmer Lines.

height (km)	emission gradient $\times 10^{-8}$ (cm^{-1})
500	1.589
1000	1.934
1500	1.900
2000	1.785
2500	1.600
3000	1.255